

The Hephaestos Proposal

Preliminary Satellite Design for the Monitoring of Urban Heat Islands

D. Petrovics and S. Ritchie

ABSTRACT

This report examines the feasibility of mounting a thermal imager and atmospheric spectrometer on a LEO satellite for the purpose of tracking the development and formation of urban heat islands, or elevated thermal zones around the cities of the world caused by human development of land. These heat islands are powerful indicators of the effect of human cities on the ongoing climate crisis, and the system proposed in this report would act as a feedback system and allow various cities to evaluate and adapt possible suggestions for the reduction of carbon emissions and the mitigation of these urban heat islands. Various important subsystems were designed based on stringent design requirements focused on the well-being of the scientific payload and a preliminary design for the Hephaestos spacecraft was proposed. It was found that Hephaestos represents a viable option for a feedback system on climate change, but much work must be done to expand this initial proposal before Hephaestos could realistically enter production as a viable commercial satellite.

Table of Contents

<u>1</u>	<u>INTRODUCTION</u>	<u>1</u>
1.1	SCIENTIFIC BACKGROUND	1
1.2	OVERALL APPROACH AND ORGANIZATION	3
<u>2</u>	<u>SYSTEMS OVERVIEW</u>	<u>5</u>
<u>3</u>	<u>PAYOUT</u>	<u>6</u>
3.1	OVERVIEW AND REQUIREMENTS	6
3.2	DETAILED DESIGN	6
3.3	FUTURE WORK	10
<u>4</u>	<u>MISSION ANALYSIS AND LAUNCH</u>	<u>11</u>
4.1	OVERVIEW AND REQUIREMENTS	11
4.2	DETAILED DESIGN	11
4.3	FUTURE WORK	14
<u>5</u>	<u>PROPULSION</u>	<u>15</u>
5.1	OVERVIEW AND REQUIREMENTS	15
5.2	DETAILED DESIGN	15
5.3	FUTURE WORK	18
<u>6</u>	<u>POWER</u>	<u>19</u>
6.1	OVERVIEW AND REQUIREMENTS	19
6.2	DETAILED DESIGN	19
6.3	FUTURE WORK	20
<u>7</u>	<u>ATTITUDE DETERMINATION AND CONTROL</u>	<u>21</u>
7.1	OVERVIEW AND REQUIREMENTS	21
7.2	DETAILED DESIGN	21
7.3	FUTURE WORK	27
<u>8</u>	<u>COMPUTERS AND SOFTWARE</u>	<u>28</u>
8.1	OVERVIEW	28
8.2	REQUIREMENTS AND DETAILED DESIGN	28
8.3	FUTURE WORK	30
<u>9</u>	<u>COMMUNICATIONS</u>	<u>31</u>
9.1	OVERVIEW AND REQUIREMENTS	31
9.2	DETAILED DESIGN	31
9.3	FUTURE WORK	36

<u>10 STRUCTURES</u>	37
10.1 OVERVIEW AND REQUIREMENTS	37
10.2 DETAILED DESIGN	37
10.3 FUTURE WORK	39
<u>11 THERMAL DESIGN</u>	40
11.1 OVERVIEW	40
11.2 DETAILED DESIGN	40
11.3 SUMMARY AND FUTURE WORK	42
<u>12 CONCLUSION</u>	43
<u>APPENDIX A: SOURCES</u>	44
A.1 REFERENCES	44
A.2 NOTES	44
<u>APPENDIX B: PROPULSION</u>	46
B.1 THRUSTER SPEC SHEET	46
B.2 PROPELLANT TANK SPEC SHEET	47

1 Introduction

1.1 Scientific Background

Urban heat islands are bubbles of heat centered about large populated areas. The primary reason for this heat has to do with urbanization and modification of the land, as well as waste heat generated by energy usage within the city. According to the EPA, “heat islands form as vegetation is replaced by asphalt and concrete for roads, buildings, and other structures necessary to accommodate growing populations. These surfaces absorb - rather than reflect - the sun's heat, causing surface temperatures and overall ambient temperatures to rise.”^[1] Furthermore, the EPA states that “displacing trees and vegetation minimizes the natural cooling effects of shading and evaporation of water from soil and leaves (evapotranspiration).” The end effect is an increase in temperature within the metropolitan area. This temperature increase is typically greatest during the evening but is also perceptible during the day. Additionally, monthly rainfall increases by about 28% as a result of urban heat islands, usually in areas several miles downwind of the city.^[2]

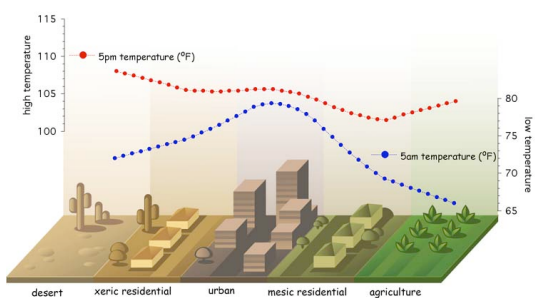


Figure 1.1: Urban Heat Island Cooling Effect.
Source:
http://asusmart.com/images/UC_figure1.jpg

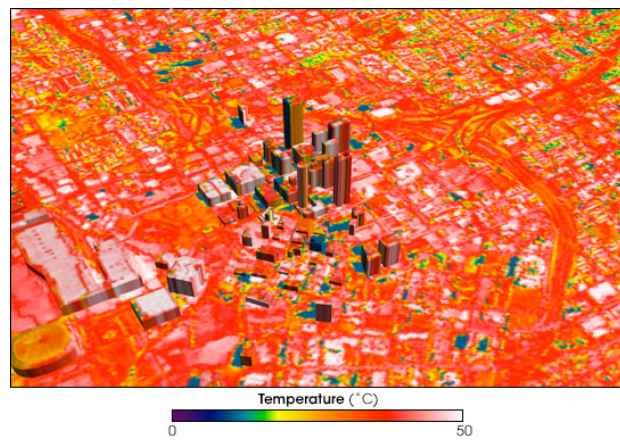


Figure 1.2: Urban Heat Island, Atlanta GA. Source:
http://en.wikipedia.org/wiki/Urban_heat_island

The main reason for retaining high temperatures in the evening has to do with manmade structures blocking thermal radiation to the sky. According to the EPA, “tall buildings and narrow streets can heat air trapped between them and reduce air flow.” Since these structures are warmer than the night sky, less heat radiates away from the ground since it is closer to equilibrium. Also, building materials such as concrete and asphalt have greatly different thermal bulk properties, such as heat capacity and thermal conductivity than natural materials^[3]. Lack of vegetation in urban areas also exacerbates this problem. Another reason for the high temperatures has to do with the ‘canyon effect,’ which states that high objects with a large surface area create many opportunities for reflection of sunlight, increasing the efficiency with which urban areas are heated.^[4] These tall buildings also block wind, inhibiting convection-cooling of the city. Lastly, the EPA warns that “waste heat from vehicles, factories, and air conditioners may add warmth to their surroundings, further exacerbating the heat island effect.”^[5]

The significance of urban heat islands is quite profound on the city's inhabitants. Health is adversely affected by the increased temperature, leading to higher rates of heat related illness and mortality. Furthermore, urban heat islands increase energy costs, decrease visibility levels and degrade the air quality of the surrounding atmosphere. A complete summary of the effect of urban heat islands on a range of variables for a mid-latitude city with 1 million inhabitants is given in Figure 1.3.

Variable	Change	magnitude/comments
Turbulence intensity	greater	10-50%
Wind speed	Decreased	5-30% at 10 m in strong flow
	Increased	In weak flow with heat island
Wind direction	Altered	1-10 degrees
UV radiation	Much less	25-90%
Solar radiation	Less	1-25%
Infrared input	Greater	5-40%
Visibility	Reduced	
Evaporation	Less	About 50%
Convective heat flux	Greater	About 50%
Heat storage	Greater	About 200%
Air temperature	Warmer	1-3 degrees C per 100 years; 1-3 degrees C annual mean up to 12 degrees C hourly mean
Humidity	Drier	Summer daytime
	More moist	Summer night, all day winter
Cloud	More haze	In and downwind of city
	More cloud	Especially in lee of city
Fog	More or less	Depends on aerosol and surroundings
Precipitation		
Snow	Less	Some turns to rain
Total	More?	To the lee of rather than in city
Thunderstorms	More	
Tornadoes	less	

Source: adapted after Oke, T.R. (1997), page 275.

Figure 1.3: Source: <http://asusmart.com/urbanclimate.php>

The exact relation of urban heat islands to global warming is not very well understood. It is clear however, that by increasing the temperature in metropolitan areas, urban heat islands increase the demand for energy dependent processes such as air conditioning. This in, turn, increases the amount of fossil fuels burned at power plants which increases greenhouse gases, the culprit behind global warming. Because of this fact, steps to reduce urban heat islands can also indirectly reduce global warming in the long run.

Another relation to global warming has to do with statistical influence of temperature readings. Many opponents of global warming argue that urban heat islands may be skewing temperature readings—meaning that the rise in temperature we have witnessed over the last few years is not necessarily an indication of global warming. Most people have argued, however, that urban heat islands are not skewing temperature readings. Experiments have been conducted comparing the temperature increase on calm days and on windy days (when the UHI effect should be mitigated), and have found that in fact the temperature increase, over time, is the same regardless of wind speed. This would indicate that global warming is behind the general increase of temperature, not urban heat islands. However, others have countered that the boundary layer heat fluxes have diurnal variations that may bias the results of the above experiment.^[6]

One way to help resolve this conflict would be through using a satellite to get more accurate temperature readings right above the cities, free from the bias of boundary

layers (which occur closer to the ground). Also, the spacecraft could study how CO₂ emissions increase in relation to temperature by studying the atmospheric makeup right above urban heat islands. (Or where the corresponding power plants are for the given city). These results could definitely prove the theory that UHI indirectly increases global warming by increasing energy demands (in turn leading to more fossil fuel consumption), while also putting to rest any theory that UHIs are skewing global warming statistics.

Similar studies have been done using NASA's Moderate Resolution Imaging Spectroradiometer (MODIS) instrument on the Terra satellite and the Thematic Mapper of the Landsat program. However, currently no satellite exists which is devoted solely to the study of urban heat islands. A successful satellite will gather images from the visible and infrared spectrums, as well as perform atmospheric analysis and gather CO₂ readings right above cities. Having a dedicated satellite would show the changes over time of each individual city. The satellite would have to pass over each city every few days, preferably always either at noon or at midnight. Temperature variations and atmospheric content changes could then be gathered over time on a city by city basis, resulting in much more knowledge about urban heat islands and their combined effect on increased energy consumption and global warming.

Currently, the only known method of reducing urban heat islands involves planting more vegetation, using cooler roofs and building materials with more environmentally friendly thermal properties. Switching from absorptive materials such as concrete and asphalt to reflective materials is also a useful tactic. Some of the best methods of reducing urban heat islands are green roofs, which increase vegetation while also decreasing absorptance. Thus, the satellite would ultimately be a way of studying urban heat island and raising awareness about their potential impacts. Since the satellite can draw data from so many different studies, a myriad of potential tactics of reducing UHIs can also be studied, confirming those methods which work best and perhaps ultimately slowing the increased energy demands of UHIs.

1.2 Overall Approach and Organization

The approach of the design team to the creation of the Hephaestos UHI Monitor began with analysis of the above scientific background above. Careful attention was then given to the type of payload and instrumentation that would characterize a mission designed to track the evolution of urban heat islands over time. As the mission is scientific, each subsystem of the Hephaestos spacecraft was designed with the well-being of the scientific payload in mind. To make sure that this goal stood clear above all others, a proper payload was crafted first around which the other systems could be designed. The payload was designed to maximize the amount of scientific data collected given the limited computing and imaging resources that every space-based system must accept.

A number of other basic subsystems were then chosen and designed to provide redundancy in computation and accuracy, precision and safety for the scientific payload. These systems are listed below under "Systems Overview". For each system a number of sub-requirements were decided upon to guide the design process. The team iterated through each system, fleshing out simple concepts for each and coming back again and again as the connections and links between each system began to make themselves clear. The final designs for each subsystem were completed with a large degree of interconnection to and dependence on each of the other subsystems on the spacecraft.

After the design of the full spacecraft was finalized, a launch vehicle was chosen to deposit the Hephaestos UHI monitor into the proper orbit decided upon in the mission analysis sub-section. Each system was analyzed in-depth using the tools appropriate to the Space System Design course (MAE 342) for which this report is being developed.

Each of the various spacecraft subsystems has been presented with an overview and summary of the system goals and requirements. After this a section is included on the detailed analysis and testing that went into the development of each final sub-system, always keeping in mind both the goals of the sub-system and the larger goals of the Hephaestos spacecraft as outlined below in section 2. As the scope of this report could not possibly include every test and analytical sequence that must be run on the spacecraft before the design could be called complete, a section on future work was included under each sub-system to detail the thought process that would have gone into a full-fledged satellite design. Also, we would like to thank Professor Kasdin for letting us employ the organizational structure of the Hermes Project, a proposal for another LEO satellite written in the spring of 2006.

2 Systems Overview

The success of the spacecraft design as a whole depends on the satisfaction of a number of requirements set by the spacecraft's constituent subsystems. These requirements are listed below.

Payload

Choose a spectral imager and atmospheric spectrometer with the proper characteristics to collect data for the formation of a 3D coverage map of the world's urban heat islands.

Mission Analysis & Launch

Design an orbit to maximize the utility of the scientific data obtained from the payload. Choose a launch vehicle suitable for placing a satellite in LEO.

Propulsion

Design a system to counteract atmospheric drag effects and maintain altitude for proper station-keeping for the duration of the mission.

Power

Generate and store power to run each of the other subsystems.

Attitude Determination and Control

Create a system which can accurately determine the orientation of the spacecraft within a defined body frame and control for any pointing errors that may evolve over time.

Computers and Software

Choose a multiprocessor and memory array to control the ADC, process data from the communications antennae and scientific payload, and buffer this data effectively.

Communications

Create a system capable of transferring data from the scientific payload to selected ground stations around the world. Design the communications link.

Structures

Design the primary and secondary structures of the spacecraft and propose an internal architecture for the other subsystems. The design must withstand the launch and orbital environments while striving for minimal volume and mass.

Thermal Design

Create a passive and active thermal control system to regulate all components and keep them within the operating temperatures defined for each component.

Within each sub-system the team strove for efficient and accurate design. The scientific payload requires that every system accomplish its objectives with a high degree of accuracy and precision so as not to interfere with any measurements being taken. Cost was kept low using off-the-shelf components and minimalist instrumentation choices.

3 Payload

3.1 Overview and Requirements

This section will develop the necessary payload to achieve the scientific goals outlined in the introduction. Namely, the satellite must have the capability of assessing the environmental effects of urban heat islands over time. This means that the spacecraft must take a large number of readings over the same city during the same time of day for an extended period of time. This section will introduce and study the two instruments that will be taking the readings. The first is a pushbroom imager that can take images of urban heat islands in both the visible and IR bands. The second is an atmospheric spectroscopy machine that is currently used on board the Aqua satellite.

3.2 Detailed Design

Pushbroom Imager

Several different imaging techniques exist, but perhaps the best tested and most popular method is a pushbroom imager. As seen in Figure 3.1., a pushbroom scanner gets its name from the fact that it moves its instantaneous field of view (IFOV) along the ground track with its array of sensors perpendicular to the track. The area array referenced in Figure 3.1 is an array of pixels that processes the image through a network of gratings and optics. Figure 3.2 shows a similar setup for a pushbroom spectrometer.

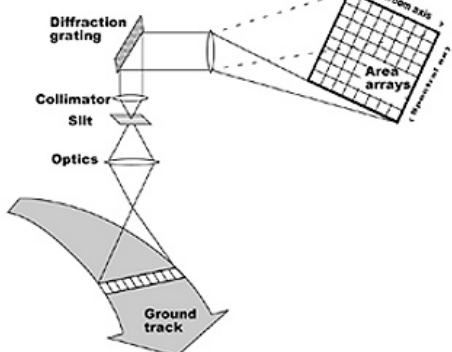


Figure 3.1:
<http://rst.gsfc.nasa.gov/Intro/pushbroomX.jpg>

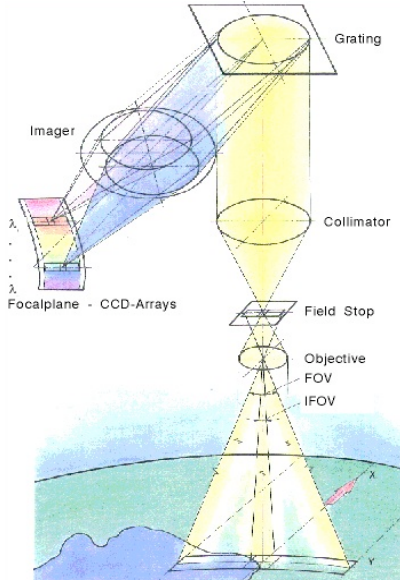


Figure 3.2: http://ceos.cnes.fr:8100/cdrom-98/ceos1/satellit/mos/jpg/abbspm_f.jpg

Choosing a Half Cone Angle for the Imager

In order to balance high resolution with relatively frequent access times, an optimization must be performed on the half cone angle of the imager. The larger this angle, the more frequently it will be able to see any given city. However, a larger angle means smaller resolution given the same number of pixels in the imager. In order to come up with a good compromise between these two factors, we used Satellite Tool Kits software (STK) to perform a coverage grid analysis. As shown in the Mission Analysis and Launch section, the ground tracks of the satellite repeat themselves every 5 days (76 orbits), so we performed a coverage analysis within that timeframe. A coverage grid was added to the project scenario covering latitudes from -55 degrees to 70 degrees, effectively spanning all of the world's major cities (see figure 3.3). The resolution of the grid was set at 1 degree. Several different half cone angles were tested, and 31 degrees was determined to be the best compromise. Figure 3.4 shows the percent coverage by latitude of the imager at this half angle. The majority of the time is centered at the higher latitudes, with the least amount of time spent near the equator.

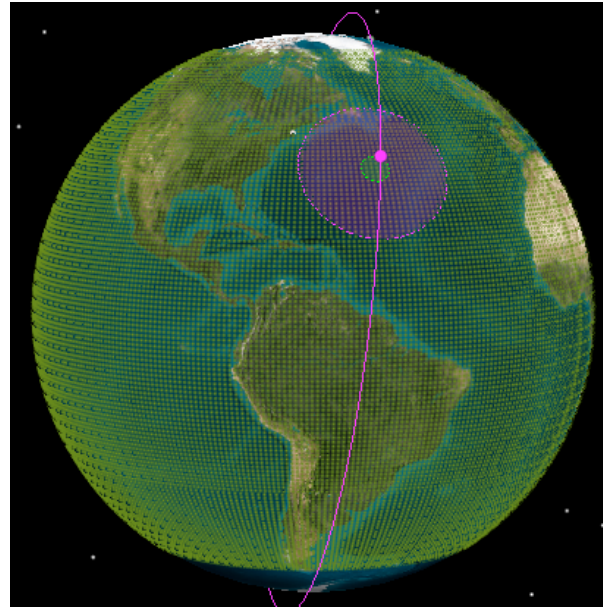


Figure 3.2: STK Global Coverage Grid

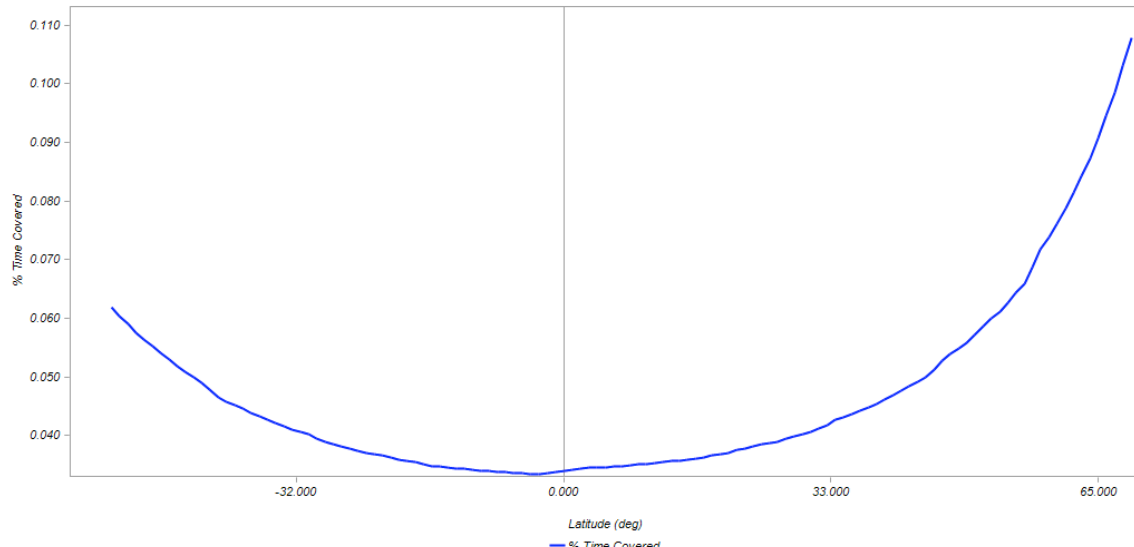


Figure 3.3: Percent Coverage by Latitude of the Imager

Finding the Resolution

Now given the half cone angle of the imager, we can calculate the swath width on the earth (by ignoring the curvature of the earth) as $2*500\tan(31)$ to obtain 600 kilometers. We then decided that, since the resolution of a pushbroom falls sharply towards the outside of the swath with, we would limit our camera field of view to 200km by 200km, and take two pictures of the city within this square (one in the infrared and one in the visible light spectrum). This could be achieved by programming the satellite with the coordinates of all the cities that we want to image, and having the imager swivel to their coordinates when the city is within the ground swath.

The infrared picture will show the distribution of heat right in and around the city, while the visible spectrum will analyze the vegetation in the area so that it may be compared to the city's heat profile (to study if there is a correlation between urban heat islands and amount of vegetation in and around the city).

In order to calculate the resolution of our image, we have to choose the size and number of the charge coupled devices (CCDs) in the spacecraft imager. Modeling our imager after the one used in the Sloan Digital Sky Survey (SDSS), we have decided to use 30 CCDs, each with a resolution of 2048*2048 pixels to achieve a total of 125.83 megapixels. Distributed over an area of 200km by 200km, this comes out to a resolution of 17.83meters/pixel, which should be fine enough for our studies.

Next, we find the velocity of the ground swath on the earth by applying a simple ratio of velocities.

$$\frac{7.66 \frac{\text{km}}{\text{sec}}}{6378\text{km} + 500\text{km}} = \frac{\text{SW}_{\text{vel}} \frac{\text{km}}{\text{sec}}}{6378\text{km}} \quad (3.1)$$

Solving for SW_{vel} yields 7.10 km/sec. Thus, if the imager takes about 1 second to take and process the picture, it will have moved approximately 7.1km out of the 200km field of view (3.55%), which could result in some blur. To solve this problem, the camera should be able to swivel just under 0.5 degrees within 1 second to ensure that the boresight of the camera is on the same point the entire time. The camera can use the same swiveling motion for this purpose as it does to select the field of view from the swath area (as discussed above).

The Atmospheric Spectrometer

Instead of designing a brand new spectrometer, we have decided to use the Atmospheric Infrared Sounder (AIRS) for our mission. The AIRS measures global climate change indicators such as water vapor and greenhouse gases. It does this by splitting infrared radiation into its constituent colors, and using the results to infer information about temperature, water vapor, and gases such as ozone, carbon monoxide, carbon dioxide, methane and sulfur dioxide.^[1] AIRS is capable of taking 325,000 measurements a day, over a range of altitudes (hence the ‘sounder’ part of the name).^[2]

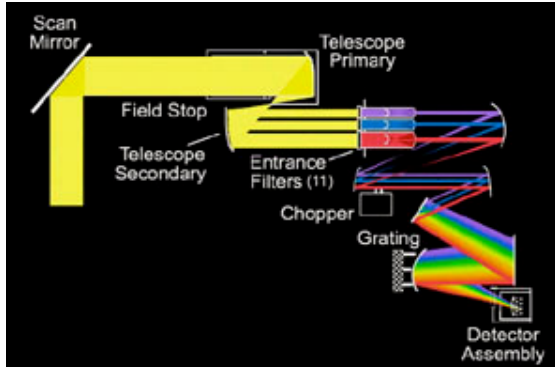


Figure 3.4: AIRS Optics. Source: Zareh Gorjian, NASA JPL



Figure 3.5: AIRS Instruments Source: NASA JPL

AIRS is currently being used on the Aquas mission and is developed by JPL. According to JPL, the AIRS “represents the most advanced sounding system ever deployed in space. The system is capable of measuring the atmospheric temperature in the troposphere with radiosonde accuracies of 1 K over 1 km-thick layers under both clear and cloudy conditions.”^[3] For our application, measurements would be taken in the troposphere (6-20km above the ground). Figure 3.7 below shows a map of CO₂ coverage over the earth at a height of 8km produced by AIRS.

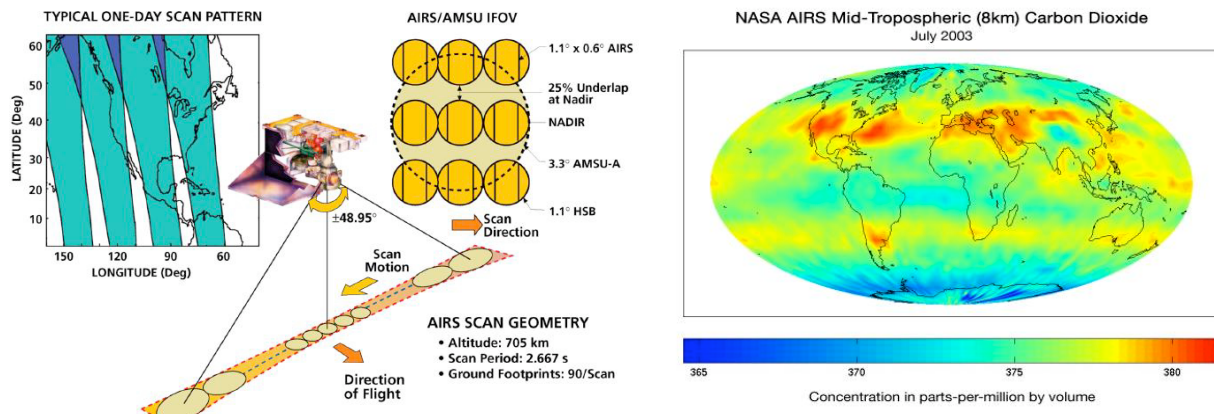


Figure 3.6: AIRS Scan Geometry. Source: JPL

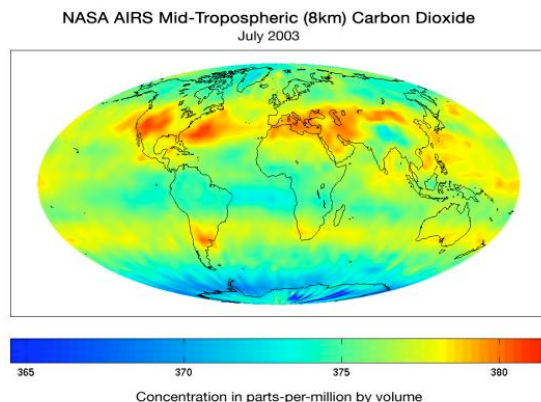


Figure 3.7: Source:
http://photojournal.jpl.nasa.gov/jpegMod/PIA09269_modest.jpg

Figure 3.4 shows how a spectrometer breaks light into its basic colors using mirrors, filters, choppers and grating. The detector assembly then analyzes the constituent wavelengths and sends the information to the computer. Figure 3.6 shows the scan pattern of the AIRS aboard the Aqua. Note than on our spacecraft, the altitude is 500km instead of 705km, so the cone angle and scan period will have to be adjusted.

From the JPL website, we have gathered the most important specifications for AIRS. The infrared spectral coverage ranges from 3.74 micrometers to 15.4 micrometers, the scan angle is 49.5 degrees about the nadir, the IFOV is 1.1 degrees, it consumes 256W of power and weighs 166kg. The lifetime is expected to last about 5 years.^[4]

3.3 Future Work

Thorough simulations must be done to ensure that AIRS can work well with the orbital parameters of our satellite, as they are slightly different than on the Aqua. We must also get a price quote from JPL and see if they are willing to make one more model. If possible, it would be helpful to get data from lower altitudes so we can associate carbon emissions with a specific city. If the altitudes in the reading are too high then it we would have a difficult time associating carbon dioxide concentrations with specific urban heat islands. For the pushbroom imager, we need to do a financial analysis on the 30 CCDs and get a more precise design for the camera, specifically the swiveling component. Specifications must be made on the camera in terms of its mass and power consumption.

4 Mission Analysis and Launch

4.1 Overview and Requirements

The objective of the Mission Analysis and Launch section is to design an orbit that meets the specifications of the mission and to select a launch vehicle that is both economical and reliable. The science specifications outlined in section 1A require a satellite with the ability to have near global coverage, high resolution visible and spectral imaging, and atmospheric spectroscopy capabilities. This section will optimize altitude, taking drag, resolution, and communication considerations into account. Sun exposure is also a factor in orbital design, and factors such as global coverage, launch window and launch site are also considered.

4.2 Detailed Design

Since the spacecraft requires high imaging capabilities in a variety of global locations, we believed that the best orbit would be an inclined, sun synchronous LEO. Creating a sun synchronous orbit involves combining the altitude and inclination of the spacecraft in such a way that it passes over the same part of the earth during the same local time. This is achieved by picking a combination of altitude and inclination that makes the orbital plane precess at about 1 degree eastward per day, simulating the earth's movement about the sun.

This is a relatively common way of designing LEO imaging satellites since it provides consistent lighting conditions. It avoids border lines when patching together visible spectrum imaging and also ensures that the thermal data will be from the same time of day. In order to get accurate data, we need to make sure that, for example, the thermal data over Los Angeles is gathered during the same time of day at every pass. We decided to create a noon-midnight sun-synchronous orbit, which means that the satellite will pass over each point and noon and midnight every day. This will give us consistent readings over each city while taking diurnal variations into account (by obtaining the reading during the same time of day and night).

Since altitude and inclination are inextricably linked for a noon-midnight synchronous satellite, we decided to optimize the altitude, which in turn would also fix the orbital inclination. In order to optimize the altitude, Doppler Shift, aerodynamic drag, and imaging resolution considerations must be taken into account. Doppler shift is caused by the fact that the satellites are moving at speeds of several kilometers per second with respect to the Earth surface. The phenomenon complicates receiver designs, widens bandwidths and lowers signal to noise ratios. The magnitude of the shift, Δf , can be computed as a function of the rate of change of the slant range as

$$\Delta f = \frac{-f}{c} \left(\frac{dR}{dt} \right) \quad (4.1)$$

where c is the speed of light and f is the transmission frequency. The formula shows that the Doppler Shift clearly increases with altitude, meaning a lower altitude is preferable from this perspective.

The aerodynamic drag force, F_D , on a satellite is defined as

$$F_D = \frac{1}{2} \rho V^2 C_D A \quad (4.2)$$

where V is the velocity of the spacecraft, C_D is the coefficient of drag, A is the frontal area, and ρ is the density of the atmosphere. Although we do not explicitly compute C_D or A here, it is common to assume a coefficient of drag of 2.5 and a frontal area of about 4m^2 .^[1] The velocity of the spacecraft is computed as the circumference of the orbit divided by the period, yielding:

$$\frac{2\pi * 6878\text{km}}{94\text{min} * 60\frac{\text{sec}}{\text{min}}} = 7.66 \text{ km/sec.} \quad (4.3)$$

Plugging into equation (4.2), we get the aerodynamic drag force as a function of density. Using the USA2000 program, we can get the density as a function of altitude, and thus also the drag force as a function of altitude. Figure 4.1 clearly shows that the drag force decreases with altitude, as expected. The aerodynamic drag on the satellite spikes heavily at around 300km, and is quite small by around 500km of altitude.

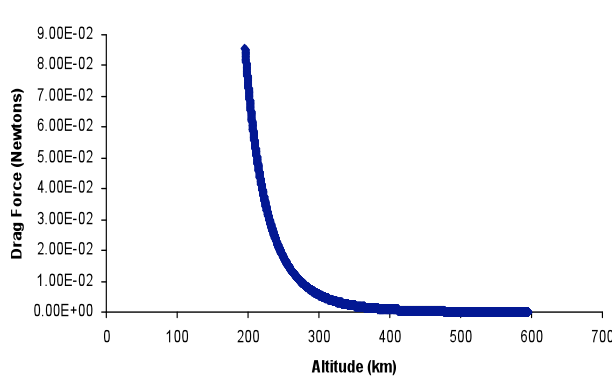


Figure 4.1: Drag Force vs. Altitude

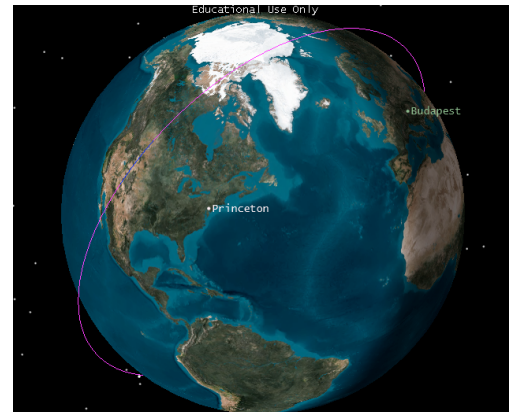
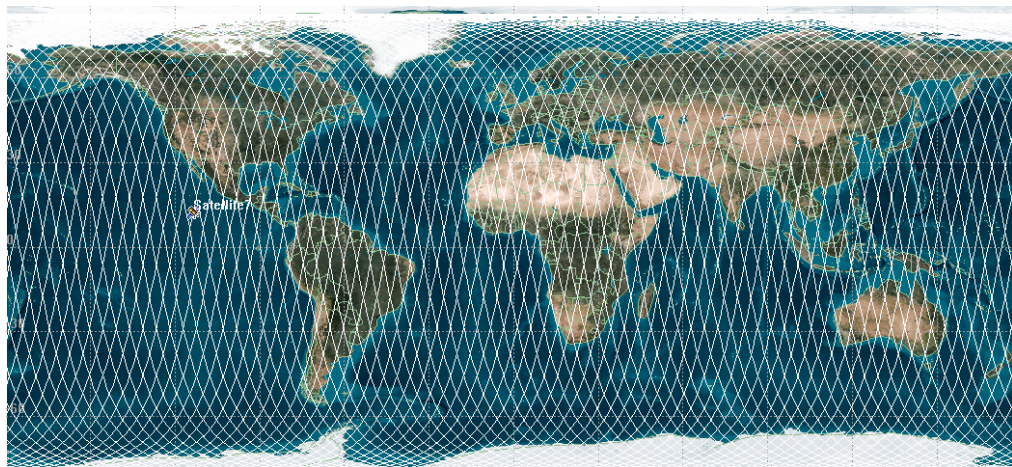


Figure 4.2: STK 3D view of LEO noon-midnight sun synchronous orbit

Magnification capabilities also go down with altitude, and given the important imaging data that is required for urban heat island imaging we have decided to give this factor extra weight in determining the altitude. We thus opted for a 500km spacecraft orbit, which is at the lower end of typical LEOs.

A 500km altitude noon-midnight sun synchronous satellite must then have an inclination of 97.41 degrees. All the relevant orbital parameters are shown in Table 4.1. A picture of the orbit in Satellite Tool Kits (STK) is also shown in Figure 4.2.

Semimajor Axis	6878.14 km
Eccentricity	0 deg
Inclination	97.4065 deg
Argument of Perigee	0 deg
Right Ascension of the Ascending Node	279.319 deg

Table 4.1: Orbital Parameters**Figure 4.3. STK 2D view of ground tracks for 5 day period**

The ground tracks of the orbit repeat every 76 orbits, or exactly 5 days, to give an orbital period of just over 94 minutes.

Station Keeping

Using Figure 4.1 and formula 4.2, we obtain the drag force on the satellite at an altitude of 500km to be approximately 1.53×10^{-4} Newtons. For a 500kg spacecraft, we have that the acceleration $a = F/m$, and the yearly velocity increment = $a \times 1$ year. This calculation yields

$$\Delta V = (1.53 \times 10^{-4} \text{ N}) / 500\text{kg} * 365\text{days} * 24\text{hrs/day} * 3600\text{sec/hr} = 9.65 \text{ m/sec/year}$$

For a 15 year mission, this would mean a total delta V of 144.75m/sec. However, in addition to this figure, smaller perturbations can arise from Solar Radiation Pressure, Luni-Solar gravitational effects as well as effects from the oblateness and the non-sphericity of the earth. However, it should be noted that the J2 effect, which stems from the oblateness of the earth, is the very phenomenon that allows sun-synchronous satellites, so in effect this perturbation is useful in that it precesses the orbital plane by one degree/day.

Launch Vehicle

We have selected the Polar Satellite Launch Vehicle (PSLV) for our satellite. The PSLV is an expendable launch system operated by the Indian Space Research Organization. It is a four stage rocket that uses both solid and liquid propulsion systems,

as well as solid rocket boosters (SRBs). Its mass is about 294,000kg, has a height of 44m and a diameter of 2.8m.^[2] It can carry a payload of 3,250kg into orbit, and it is specially designed for polar LEO, which is perfect for our application. The PSLV has been used for a number of applications, including Israeli spy satellites and German scientific satellites.^[3] In April of 2008, the PSLV successfully launched 10 satellites at the same time; a similar approach would allow for our spacecraft to share the launch cost with a number of different agencies, drastically reducing mission cost.

Launch Window and Launch Location

Most of the PSLV launches take place in Sriharikota, which is a small barrier island off of the southern coast of India. It is the location for all of India's satellite launches and home to the Satish Dhawan Space Centre (SHAR). It takes the PSLV about 12.85 minutes to enter LEO, so we must launch the satellite about 13 minutes right before noon or midnight to ensure that it enters a noon-midnight sun synchronous orbit.^[4]

Orbital Environment Considerations

Besides aerodynamic drag, the other possible perturbations may have small effects on the satellite, and they are discussed in the station keeping section. The only other serious environmental consideration is Radiation. Radiation in low earth orbits is quite low since the majority of the Van Allen Belts is above this range, located primarily between LEO and GEO orbits. Thus, although no in depth calculation is presented here it is relatively well documented that only single event upsets occur in LEO satellites, and it is very rare to have serious radiation problems.

4.3 Future Work

Future work would include assessing the viability of the launch vehicle financially and politically (since it is an Indian manufactured launch vehicle). A fairing design should also be chosen for the satellite during launch. Although it is clear that all the major cities can be covered with our spacecraft, more in depth coverage analysis should be completed for the satellite. The launch window and launch azimuth should be computed to ensure a noon-midnight sun synchronous spacecraft. Lastly, more in depth consideration should be given to aerodynamic drag effects and altitude optimization.

5 Propulsion

5.1 Overview and Requirements

The primary objective of the propulsion subsystem is to provide altitude station-keeping for the satellite. The low-earth orbit chosen to satisfy our mission requirements subjects the spacecraft to a significant amount of aerodynamic drag at the edge of the upper atmosphere. At the chosen circular orbit at 500 km altitude, loss of 20m per orbit, allowing for fluctuations in local atmospheric density, was expected. The scientific payload depends quite heavily on a constant altitude; the system was designed with multiple, redundant systems so as to minimize the possibility of failure in case of malfunction of the gyroscopic mechanisms of the attitude control system. The circular orbit also dictated that altitude corrections be applied through impulsive maneuvers at the Earth's poles, when the attitude of the spacecraft is ideal for correcting torques to be applied.

This section outlines the design procedure and final requirements for the propulsion system of the spacecraft and identifies currently available hardware solutions to the design requirements raised above.

5.2 Detailed Design

The design process began with selection of a combination of thrusters and propellant that could provide accurate altitude station-keeping with a minimum of fuel expenditure or mass penalty on the entire system. The thrusters need to provide low thrust at high cycles, perhaps once every orbit. These requirements narrowed the choices of possible systems down to either cold gas thrusters or a monopropellant thruster. Cold gas thrusters were ruled out due to their poor mass fractions and very low Isp. Using nitrogen gas, Isp of only 68 seconds^[1] is typical. This is too low to satisfy the criterion of reliability. Monopropellant hydrazine thrusters were chosen for the altitude station-keeping propulsion system, as they are one of the most common systems available and satisfy each of our requirements set out above. The fact that many systems currently in production use hydrazine thrusters guarantees low cost and mitigates the need for production of custom thrusters for this specific mission. Hydrazine in particular was chosen due to its relative stability to other monopropellants, such as hydrogen peroxide.

Hydrazine monopropellant is stored as a liquid and provides thrust through catalytic decomposition from N₂H₄ into nitrogen and hydrogen gases. This extremely exothermic process provides high Isp (210-260s) with a large range of thrust values, requires no ignition, and functions in the presence of a catalyst such as iridium. As a liquid it can be stored at very low volumes and masses. It is a known carcinogen, but this propulsion system is designed to operate only in orbit and will not present any environmental risks. In other spacecraft hydrazine has been stored safely in sealed tanks for over fifteen years^[2], satisfying our reliability criterion.

Due to the strict requirements on precise altitude control defined by the scientific payload, the liquid hydrazine propellant must be controlled by a propellant management device to ensure constant thrust as the supply bloods out. Of all of the various solutions for propellant management, a satellite propellant bladder tank pressurized with gas from an external tank was found to be most appropriate for altitude control. The system

controls hydrazine delivery by storing the propellant inside an elastomeric diaphragm located inside a rigid fuel tank. The interstitial space between the diaphragm and the tank can be filled with pressurized gas to control liquid hydrazine delivery with great accuracy. A section of a generic bladder tank is shown in figure 5.1:

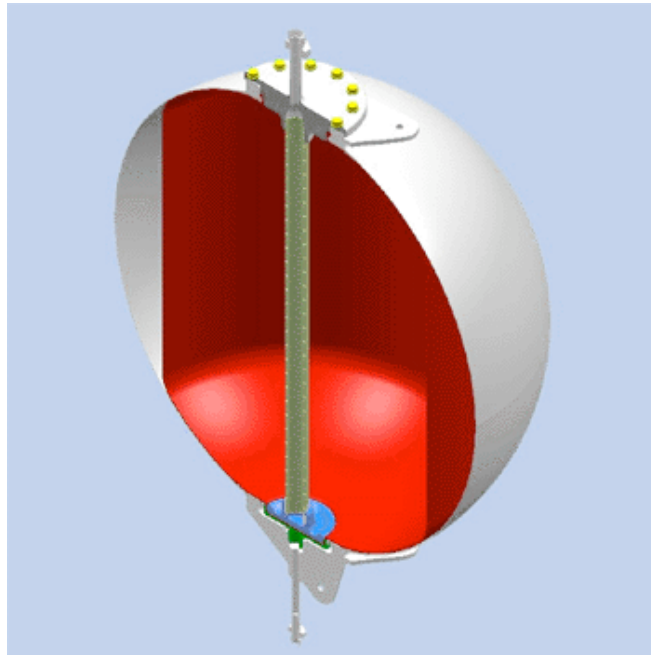


Figure 5.1: Section through Bladder Tank^[2]

The propellant delivery system could be made simpler by utilizing a bladder tank in blow-down mode, which negates the need for an external pressure tank by locking in a fixed mass of propellant gas and letting the elasticity of the internal diaphragm supply the positive pressurization force. The most pertinent drawback to the blow-down implementation is the diminishing thrust over time, due to a decrease in pressure as propellant leaves the tank. In either blow-down or pressurized modes, the diaphragm configuration provides minimization of propellant residuals and availability of propellant regardless of satellite orientation or acceleration^[3].

The propellant mass needed over the lifetime of the mission was determined using the drag force calculated in mission analysis along with a number of other quantities to be defined. F_D was found to be constant and equal to 1.53E-4 N in magnitude. The total ΔV for the mission with respect to drag was calculated to be 144.75 m/s and the Isp was 220s. The mission analysis section calculated the orbital period to be 5640 seconds. The equations below were used to calculate the total burn time and hydrazine thruster exhaust velocity:

$$I = F_D \tau_{orbit} = 2T \Delta t_{burn} \quad (5.1)$$

$$\Delta t_{burn} = \frac{F_D \tau_{orbit}}{2T} \quad (5.2)$$

$$u_{ex} = I_{sp}g_0 \quad (5.3)$$

These equations led to a burn time calculation of 0.434 seconds, at 1N thrust. The exhaust velocity was calculated to be 2158.2 m/s, with $g_0 = 9.81$. Plugging these numbers in below, along with a drag coefficient of 2.5, a frontal area A of 4 m^2 , a t_{total} of 15 years, or 473,353,890 seconds, an orbital velocity of 7.66 km/s and an atmospheric density ρ at 500km of $5.215\text{E-}13 \text{ kg/m}^3$ a total propellant mass was calculated:

$$T = m_p t_{total} u_{ex} \quad (5.4)$$

$$m_p = \frac{F_D}{u_{ex}} t_{total} = \frac{\frac{1}{2} \rho V^2 A C_D t_{total}}{I_{sp} g_0} \quad (5.5)$$

The final propellant mass was found to be 33.56 kg. Using the density of hydrazine (1.01 g/mL)^[4], the propellant tank volume was calculated to be 33.23L. Based on this requirement for the size of the pressure vessel, a propellant diaphragm tank was chosen from Pressure Systems Inc. Part 80486-1 (Appendix B.2) holds a propellant volume of 45L within a spherical tank of 484mm diameter, which provides 35.4% extra room for propellant over the bare minimum requirements.

The pressurant gas tank was then chosen by calculating the volume of pressurant gas required to create a positive pressure gradient between the residual gas left in the pressure gas tank and the final volume within the propellant tank. Helium was chosen as the pressurant due to its low molecular weight and inert properties. The actual determination of a model number for the pressurant gas tank falls beyond the scope of this report, but the addition of a separate tank for pressurant gas is not prohibitively expensive in terms of mass or volume within the spacecraft.

The specific hydrazine thruster hardware was chosen based on the above calculations for mass expulsion and a requirement for high thruster cycling, to correct for altitude once every orbit. From above, the expected impulse requirement of 0.86 N*s dictates a minimum impulse below this value. EADS model CHT-1 (Appendix B.1) was chosen to provide 1N of thrust. The Isp is 220s and the minimum impulse is below 0.01 N*s, far below the current tolerance requirement.

The final decision to be made for the propulsion system is the specific placement of the thrusters. It was decided above in mission analysis that altitude station-keeping only required acceleration along the velocity vector if the impulse was applied at the appropriate time within the spacecraft's orbit. For redundancy four thrusters were placed at the trailing end of the spacecraft with respect to the velocity vector. By placing a thruster at each corner of the rearward-facing surface the thrusters could be fired in alternate pairs oriented along opposing diagonals, allowing each pair of thrusters to conduct orbital maintenance once every two cycles. For a lifetime of 15 years, this translates to 83928 orbital cycles, or 41964 cycles per thruster pair. This falls well within the tolerance of 59000 cycles allowed per thruster pair.

5.3 Future Work

The propulsion system outlined above is very basic—much more research would need to be conducted before the system could realistically serve on a spacecraft. A system for delivery control of the propellant would need to be designed, to sit between the thrusters and the diaphragm tank chosen above. Only one axis of control was deemed necessary for the success of the mission, but further analysis of the torques on the vehicle could highlight a requirement for more degrees of control, which would increase the complexity of the thruster system and change the amount of propellant required. These decisions would lead to a determination of a final geometry of the propulsion system within the final spacecraft, which would allow for sourcing of various feed lines, sensor cables and actuator cables, along with performance indices for each of these. This report assumed that fuel transfer through feed lines would be perfect and without fluid effects, but true analysis would need to be conducted before this assumption could be trusted. The propulsion system would also need to be integrated, through controllers, with the attitude control and positioning system so as to regulate the strength of the impulsive corrections and the timing of these maneuvers.

6 Power

6.1 Overview and Requirements

This subsystem is responsible for providing power for the entire satellite. This means collecting energy from a power source such as the sun, storing it with onboard batteries, and channeling this power to other subsystems as needed. Reliability is extremely important in designing a power system as even a short interruption in power could cause the thermal systems or the imagers to fail. The Electrical and Power System accounts for up to 30% of the satellite's dry mass, so sizing and battery choice is also an important part of optimizing the design. The EPS architecture depends primarily on power loads and eclipse times, and a rough analysis is presented in this section.

6.2 Detailed Design

The power system consists of a primary energy source, an energy converter, energy storage and regulation and distribution.^[1] These various subsystems are analyzed in this section and design recommendations are made.

Energy Source

There are numerous energy sources used on satellites, including Radioisotope Thermoelectric Generators (RTGs), which operate using nuclear power, and solar cells, which operate using the photovoltaic effect. RTGs are more useful in deep space applications where solar power is less available, so they are not a good option for our spacecraft. Solar arrays can produce from 2kW to 15kW of power in GEO, and similar numbers are possible for low earth orbits.^[2]

Several different types of cells can be used in solar cells. These include, in order of increasing efficiency: Silicon, Gallium Arsenide, Dual Junction, Triple Junction, and Quad junction.^[3] The best option for our spacecraft would probably be one of the multi-junction solar cells, which are produced by Spectrolab Inc and EMCORE Corporation in the United States.^[4] These solar cells are then arranged into arrays through series-parallel grouping. The arrays are then mounted to flat substrates called panels, which are then grouped together and structurally reinforced to form a solar wing. Solar Wings must be continuously adjusted to make sure that they are facing the sun. Solar Array Drive Operations (SADA) are used to keep the solar wings pointed in the correct direction. The exact number of solar cells and the nature of the SADA depends on the power profile of our entire satellite, and is left for future research.

Energy Storage

The next step after energy generation is storage. Batteries are used to contain the energy collected by the solar cells and store for use by the rest of the satellite. There are several different types of batteries, including Nickel Cadmium, Nickel Hydrogen, Lithium Ion. The best option for our battery is Lithium Ion, since they have only half the mass of NiH₂ batteries, and one third of the volume. Their capacity and charge rate is comparable to other batteries. However, Lithium Ion batteries require external circuitry to make sure that the cell voltage is kept between 2.7V and 4.1V.^[5] Other features which may need to be optimized include charge rate, self discharge and trickle charge. In order to reach the

higher voltages needed by the bus, several Lithium Ion cells are put into parallel to increase their effective voltage.

In order to compute the necessary battery capacity, load powers and eclipse times for the spacecraft must be calculated. A noon-midnight sun-synchronous orbit will have periods of darkness every half orbit. The maximum eclipse time is approximately equal to the average eclipse time of 47 minutes (half the orbital period). This means we will need to have some extra battery storage capability to ensure that we have enough power even during periods of darkness.

$$\text{Battery Capacity} = \frac{(\text{EclipseLoadPower}) * (\text{LongestEclipseTimeInHours})}{(\text{AvgBatteryDischVoltage}) * (\text{BatteryDOD})} \quad (6.1)$$

Power Management and Distribution

The Power Management and Distribution system performs key functions such as solar array control, battery charge and discharge control, and power distribution (LM presentation). Several different architectures are available, including unregulated buses, sunlight regulated buses, and fully regulated buses. An unregulated bus is typically used on low power applications; the solar array power is modulated to match battery charge requirements. On a sunlight regulated bus, the bus voltage is regulated to account for sunlight levels and eclipses. On a fully regulated bus, the bus is regulated for sunlight and a power converter is utilized to adjust battery voltage. This is the most optimal solution, but it is also quite heavy and complex to maintain.

We have decided to use a Direct Energy Transfer, sunlight regulated bus for our spacecraft. We chose the sunlight regulated bus because it provides a good balance of power and reliability for our application. It is a direct energy transfer system, meaning that there are no active components between the solar array and its load. We will also employ a shunt controller in parallel between the solar panels and the battery which will control the voltage and dissipate any extra current not needed by the batteries.

Peak power numbers are needed to pick nominal voltage for the bus. According to Pisacane, most satellites with power usage under 1500W will use a nominal 28V bus.^[6] However, higher power GEO satellites can use up to 100V. A specific power budget needs to be performed once specific models are chosen for the various subsystems (communications antennas/transponders, attitude control mechanisms, computer chips and storage devices, thrusters, atmospheric spectrometer, the imager, etc).

6.3 Future Work

Although the basic outline for the Electric and Power Subsystem is outlined above, a more detailed architecture must be developed. This includes choosing battery chargers and regulators, defining a precise bus voltage and battery capacity. These results will be dependent upon the power budget of the entire satellite, which can be tabulated once specific equipment models are chosen for the other spacecraft systems.

7 Attitude Determination and Control

7.1 Overview and Requirements

The attitude determination and control (ADC) system is responsible for maintaining proper orientation of the spacecraft within its defined body frame so as to keep the scientific payload and communication antennas pointed in the proper direction towards earth, along the nadir vector, to collect data and communicate with ground stations. The control system is also responsible for proper orientation of the Solar Array Drive mechanism, so that the spacecraft's solar panels are always oriented towards the sun for power collection. These two requirements must be achieved with a high degree of precision and accuracy, as attitude of the spacecraft has a large effect on the orientation of the boresight of the thermal cameras for scientific data collection and the ground station communication antennas. The ADC system utilizes a number of sensors using various control laws and much electronic hardware to control the spacecraft's numerous actuators and accomplish precise orientation, meeting the above two requirements.

This section examines the various methods of attitude determination and control available to the design team and selects the most pertinent and effective options with respect to the mission requirements outlined above.

7.2 Detailed Design

Before in-depth analysis of the systems required for correct attitude determination can be undertaken several reference frames must be defined to aid in description of the orientation of the satellite. The first of these is the geocentric inertial reference frame, in which all scientific measurements will be taken so as to compile a three-dimensional model of the earth. Attitude measurements will not be taken in this reference frame, as the evolving nature of the sun-synchronous orbit within the inertial frame is not intuitive by any means and would be difficult to track with a controller.

The second reference frame is a polar frame with the radial vector r_1 pointing from the center of the earth (the origin of the inertial reference frame) out towards the satellite at any given time, r_2 pointing in the direction of the spacecraft's velocity and r_3 pointing in the direction of the right-handed orthogonal complement to the first two vectors.

The third and final reference frame is the satellite body frame. This frame is anchored to the satellite itself and fixed in such a way that, when the spacecraft is on station, any deviation from the defined reference frame represents a pointing error that can be controlled for using the systems to be designed below. The b_3 axis is lined up along the antenna, the b_1 axis points along the solar panel axes and the b_2 axis is perpendicular to these first two. With these definitions rotation about vectors b_1 , b_2 , and b_3 refer, respectively, to roll, pitch and yaw.

Assuming proper control of altitude through the hydrazine thrusters designed above, the only oscillation required through the control system is yaw, since the chosen orbit does not have an inclination that matches up perfectly to the inclination of the ecliptic plane—any sort of oscillation away from the initial conditions set up using the body frame will result in a decrease in power. Since control of these oscillations at one cycle per orbit would require almost constant control of yaw, it becomes beneficial to

sacrifice perfect attitude control and accept a penalty in power. The power subsystem was designed such that the panels would not be expected to operate at their rated optimal power outputs. With this requirement in mind it becomes enough to control for any oscillations that might develop in the roll and pitch directions, while allowing the yaw oscillations to develop but keeping them centered around the desired point. The most important characteristic for the spacecraft control system is damping of oscillations of the scientific payload.

The two branches of control examined were full three-axis control and various de-spinning techniques using momentum wheels and gyroscopic effects. De-spinning does not make sense, as the complexity of the de-spinning platform would be prohibitively massive and complex. Below some methods of three-axis attitude determination available to the current spacecraft are considered.

Magnetometer

A magnetometer determines orientation within the body frame by passing an AC current through a single coil adjacent to a magnet. The electromagnetic current induced in the magnet induces another current in the second coil within the system—the variation between the two currents, induced and applied, can be used to determine the orientation of the magnetometer within the earth's magnetic field. Three axes within the device are required to place the spacecraft within the earth's inertial reference frame. The magnetometer is very useful in this application as the magnetic sensing can be achieved using magnetic torque rods, which are very effective in controlling the three spacecraft axes. A magnetometer and a depiction of the earth's magnetic field is shown in figure 7.1.

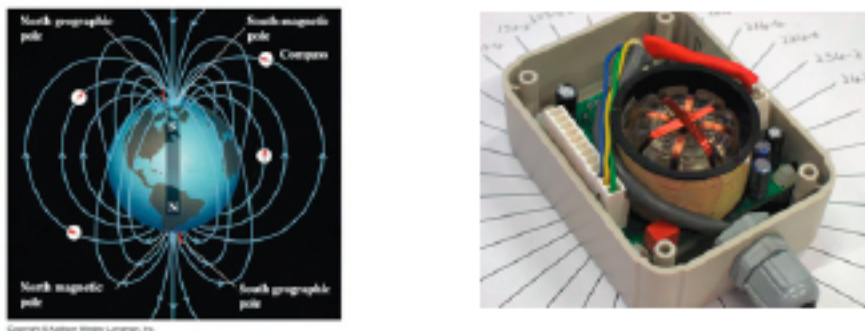


Figure 7.1: Attitude Determination using Magnetometers

Two-Axis Sun Sensor

The two-axis sun sensor can be used to measure the elevation angle and azimuth of the sun through the use of a transparent block of material with a known refractive index n painted with an opaque coating. The light of the sun passes through a slit in this opaque coating, and the difference in position between the original slit and the projected slit allow for calculation of the above measurements. This method does not provide determination of the spacecraft's radial distance from the sun, so further methods of attitude determination will be required. A single-axis sun sensor is pictured in figure 7.2.

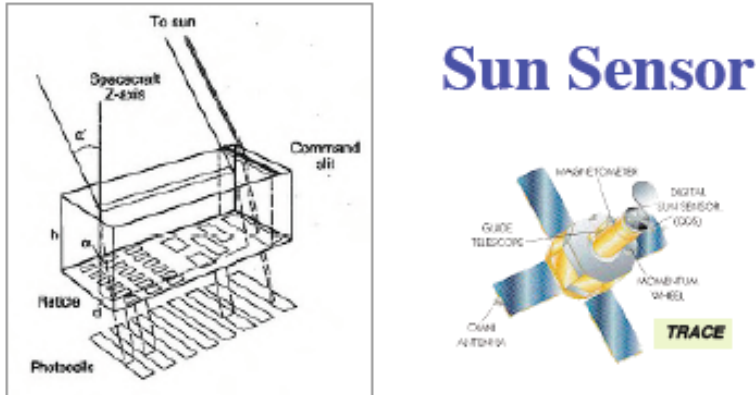


Figure 7.2: Sun Sensor Diagram

Static Horizon Sensor

The static horizon sensor consists of a ring of infrared photodetectors which can sense the circular horizon of the earth, locating the nadir direction relative to the spacecraft's body axes and aligning the body frame with the polar frame defined above. Used in conjunction with the two-axis sun sensor this sensor allows for complete determination of attitude within earth's inertial reference frame. The two types of horizon sensors considered were active and static—the active system is unnecessarily complicated for this application, as the scientific payload needs only to be pointed along the nadir and enough other simple sensors will be present on the spacecraft that a static horizon sensor, incapable of will be able to function appropriately. A schematic and photograph of the sensor is shown in figure 7.3.

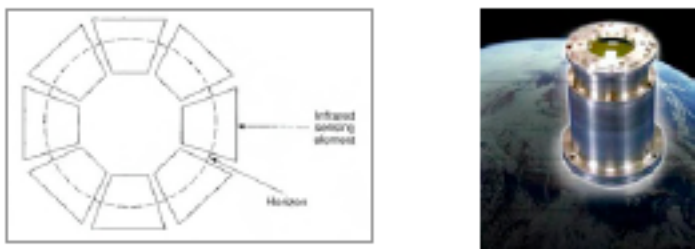


Figure 7.3: Static Earth Horizon Sensor

GPS Receiver

The GPS receiver is necessary in this application in that it allows for accurate determination of position, velocity and acceleration of the spacecraft, as well as a rough measurement of attitude when the other sensors are inoperable, allowing for a controlled adjustment of orientation to get these other sensors back on track. Accurate knowledge of spacecraft position, velocity and acceleration is necessary for calculation of Doppler shift, which is in turn necessary for accurate communication with the ground stations during the lifetime of the mission.

Star Sensor/Tracker

The star sensor works by comparing an internal star catalogue with the Cartesian coordinates of stars on the focal plane of the sensor. This is the most accurate and complex method of attitude determination, and is far too complicated for the current spacecraft.

Next, some methods of three-axis attitude control are discussed with an eye towards systems tolerant to high cyclic frequencies.

Reaction Wheels

Reaction wheels are flywheels with a nominal angular speed of zero—when oriented in the direction of an axis the reaction wheels can take external torques on the system and, using angular acceleration, reorient the satellite while storing the external torque as an angular velocity on the reaction wheel^[1]. As the nominal velocity is zero, a separate method must be employed to bleed this angular velocity after a certain period of time. For this application multiple reaction wheels are used oriented along each body axis to provide full three-axis control. A cross section of a typical reaction wheel is shown in figure 7.4.

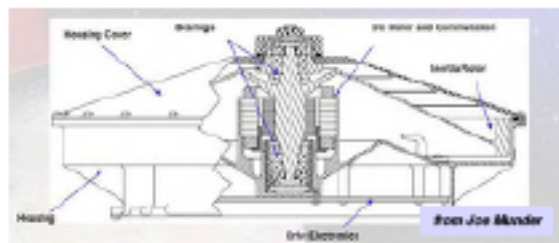


Figure 7.4: Reaction Wheel Cross-Section

Magnetic Torque Rods

The magnetic torque rods function, in addition to their role in attitude determination in the magnetometer, as the spacecraft's method of ejecting momentum built up within the reaction wheels out into the environment. By applying a current to the torque rods placed along each of the three principal body axes an external torque acts on the system and the reaction wheels can be despun to their nominal angular velocity of zero. A number of torque rods are shown in figure 7.5.



Figure 7.5: Various Magnetic Torque Rods

Reaction Control Thrusters

Reaction control thrusters can be used to directly control the attitude of the spacecraft by exerting an external torque on the system. In the section on propulsion the use of hydrazine thrusters for altitude station-keeping was discussed. It was that three-axis control using an RCS system would be far too complex for the current spacecraft's requirements.

The next step in design of the attitude control system is to analyze the disturbances and torques that could affect the spacecraft in the LEO environment. The primary torques to consider are the aerodynamic torque:

$$\tau_{\text{aero}} = \frac{1}{2} \rho V^2 C_D A (\mathbf{u}_v \times \mathbf{r}_{cp}) \quad (7.1)$$

where ρ is the atmospheric density at altitude, V is the orbital velocity, C_D is the drag coefficient, A is the spacecraft's frontal area, \mathbf{u}_v is the vector along the spacecraft's velocity, and \mathbf{r}_{cp} is the vector from the center of the earth to the spacecraft, along the radius of the polar frame defined above; the gravity gradient torque:

$$\tau_{gg} = \frac{3\mu}{R^3} \mathbf{u}_e \times (\mathbf{I} \cdot \mathbf{u}_e) \quad (7.2)$$

where μ is the earth's standard gravitational parameter, R is the distance of the spacecraft along \mathbf{r}_{cp} , and \mathbf{I} is the spacecraft inertia tensor; and torque induced by solar radiation pressure:

$$\tau_{SRP} = \mathbf{r} \times \left[\frac{(1+K) I_s A_{\perp}}{c} \right] \quad (7.3)$$

where K is the spacecraft surface reflectivity, \mathbf{r} is the vector along the spacecraft normal (from the center of mass to the center of pressure), I_s is the sun's intensity (1358 W/m^2 at 1 AU), c is the speed of light ($2.9979 \times 10^8 \text{ m/s}$), and A_{\perp} is the spacecraft projected area normal to the sun vector^[2].

The only torques that could reasonably arise internal to the system result from thruster misalignments:

$$\tau_{\text{thruster}} = \sum (\mathbf{r}_i \times \mathbf{T}_i) \quad (7.4)$$

where \mathbf{r}_i is the moment arm of the thruster off of the center of mass and \mathbf{T}_i is the thrust, in this application equal to 1N per thruster; and from the dipole effect of the spacecraft with regard to the magnetic field of the earth. To calculate these moments a full spacecraft model or simulation would need to be constructed. Such analysis is far beyond the scope of this project.

Assuming a spacecraft reflectivity of 0.4 based on typical values of examples within Pisacane's *Fundamentals of Space Systems*, the SRP torque was found to be cyclical from 2.535E-5 Nm to -2.535E-5 Nm depending on spacecraft orientation with respect to the sun. The gravity gradient torque was found to be, without any calculation of the inertia tensor due to a lack of detailed modeling capability, to be on the order of 3E-15 Nm to -3E-15 Nm, orders of magnitude less significant than the SRP torque. The aerodynamic torque was found to be on the order of 1.53E4 and constant. Thruster misalignment, assuming excess power of 5% and a misalignment of 0.1 meters, provides the single largest torque on the system at 5E-3 Nm. As this final torque could affect pitch and yaw, and the other torques each affect all three axes within the body frame depending on satellite orientation in the inertial reference frame, this analysis confirms that full three-axis control is indeed necessary.

From the solutions outlined above, the most simple and economical choices for attitude determination were the two-axis sun sensor, the static horizon sensor and the GPS receiver for Doppler shift calculations. A magnetometer was also selected as the magnetic torque rods included in the system allow for bleeding off of internal torques. For attitude control, these magnetic torque rods work in conjunction with a set of reaction wheels oriented along each body axis for correction of pointing errors, once the initial conditions of the system have been set. The reaction control thrusters discussed in the propulsion section will do much to counteract the effects of atmospheric drag on spacecraft altitude, and will also be useful in orienting the spacecraft at the start of its mission so as to set up proper initial conditions for the other attitude determination instruments.

The next step in development of the attitude determination and control system is a detailed analysis of the final structure so as to determine the characteristics of the various spacecraft plants. The two plants that must be controlled are the spacecraft attitude control gyros and the solar array drive mechanism, not sourced in this paper, which controls the angle of the spacecraft's solar panels. An observer-based feedback system will be utilized rather than a full-state feedback system, as system reliability is more important to the mission than conservation of power or computational intensity, and a full-state feedback system, though more accurate, could potentially involve many, many states and according sensors. Failure of one of these sensors could jeopardize the mission. Observer-based feedback allows for fewer sensors and redundancy between these. Development of the actual closed control loop to keep the spacecraft on track and reject disturbances introduced by the torques mentioned above falls beyond the scope of this report. Due to the lack of restraint on computational intensity, the coordinate system of the spacecraft will be programmed using quaternions^[3] rather than Euler angles, as the latter must be linearized about an equilibrium point and hence would require complex calculations and multiple dynamic models to orient the satellite to its required initial position.

7.3 Future Work

Before the attitude determination and control system could function in an operational spacecraft much work would have to be done beyond the research conducted above. The attitude control system would need to be able to account for multiple operational modes. The control loop described above would only provide reference tracking when the spacecraft was on station, and would not be able to control the spacecraft during the initial orientation phase, on orbital insertion. Multiple control modes would have to be developed for situations such as this; other disturbances that must be accounted for could be misfired thrusters, or reaction wheels that were not de-spun properly and have reached saturation. Impacts of various vibrations and correction errors on the scientific payload would need to be considered in the selection of the final attitude control hardware, as well as the computational requirements of various other attitude control systems not considered in this report. The final control loop itself would need to be tested under a variety of conditions to ensure that the observer-based negative feedback system could track errors and noise with a significant degree of redundancy and disturbance rejection.

8 Computers and Software

8.1 Overview

The computer and software system is responsible for collection of data from the scientific payload, proper storage and routing of this data through the spacecraft's central processor for analysis, and coordination of the attitude determination and control system through its various microprocessors and controllers. The computer system also needs to coordinate communication with the ground and control for proper data transmission during the lifetime of the mission. This section will calculate various data throughput rates for communication, control and storage of scientific data, and will then choose components able to handle potential full load computer requirements.

Many of the satellite subsystems involved in an earth-sensing mission have a negligible draw on system resources and computing power, and have been neglected in the following calculations of processor requirement with the understanding that a large factor of safety will cover the omission.

8.2 Requirements and Detailed Design

The first step in the design of the computer and software subsystem was the choice of a multiprocessor capable of handling the large streams of data from both the scientific payload and the downlink and uplink antennas. In the payload sub-section, the maximum data download rate from the scientific payload was calculated to be 347.4 Mbps, which is the limit for downloading all memory from onboard flash drives down to the ground at maximum buffer load. The engineering data download data rate was assumed to be 100 Mbps; this is, based on the group's experience with computing hardware, far in excess of the actual rates that will be encountered during the spacecraft mission, but as in-depth analysis of the content of the spacecraft's communications with the ground stations chosen above is beyond the scope of this report, a generous margin of error was included. Finally an additional 1 Mbps was included to accommodate ADC processes, as determined in the section on attitude determination and control.

Assuming a 32 bit CPU, The processor speed must be able to accommodate $(448.4 \text{ Mbits/second}) / (32 \text{ bit CPU}) = 14.01 \text{ MHz} = 140.1 \text{ MIPS}$, assuming a conversion factor of $(1 \text{ MIPS} / 1 \text{ MHz})$, as can be found on many common computer processors^[1]. As these are only estimates, a safety factor of 2 pushes the requirement for processor speed to 280.2 MIPS.

The market of commercially available space-computers and processors was difficult to penetrate, as many current spacecraft applications rely on custom computers. This project's design criteria aims for a reduction in cost through the use of off-the-shelf components—the only multi-processor currently in production that could be identified was the Harris CrossStar-97 Multiprocessor, a 32-bit CPU array capable of delivering over 350 MIPS, which falls well above the requirements along with their large safety margin^[2]. This spacecraft design team chose to innovate on the Harris CrossStar-97 by investigating an alternative option, the Dependable Multiprocessor, currently being developed by Honeywell, Inc. as a part of the New Millennium Program at NASA^[3].

The Dependable Multiprocessor seeks to provide far more processing power per watt than any multiprocessor in use today, due to the massive communications loads

imposed on spacecraft processors and memory banks by the burgeoning resolution of state-of-the-art spectrometers. Field Programmable Gate Arrays are used as accelerators to give anywhere from 100x to 1000x improvement in data throughput rates over traditional solutions such as the Harris CrossStar.

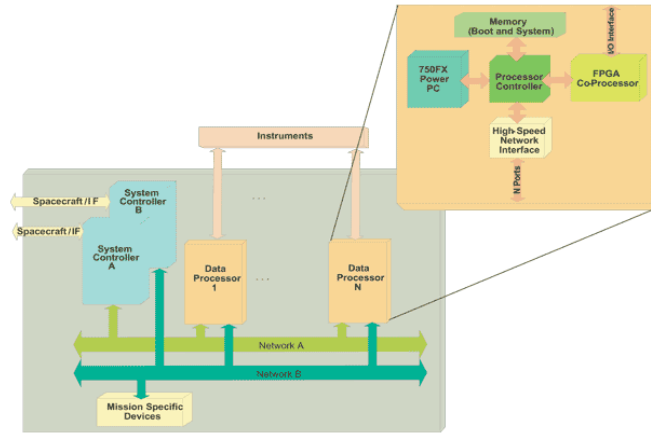


Figure 5.1: Hardware Architecture of Dependable Multiprocessor^[4]

The Dependable Multiprocessor was also favorable for its design as a spacecraft system and resulting radiation shielding. The hardware architecture of this system is shown above in figure 5.1. The design criteria for the multiprocessor specify a goal of 300 MIPS/watt of power. This astonishing figure would allow the spacecraft to satisfy the power requirement of the CPU array with a single watt of power.

The next goal of the computing team was to choose a suitable processor module. The Harris CrossStar documentation makes reference to the RH3000 chipset, which consists of the RHC3001 CPU and the RHS3010A FPU. The current spacecraft cannot utilize this chipset without accepting the entire Harris system, and is currently waiting on more documentation on chipset being developed by Honeywell, Inc. as part of the Dependable Multiprocessor package. The chipset should be fully radiation-hardened so as to withstand the difficult conditions of low-earth orbit or electronic devices. It should also be immune to latch-up, meaning that the space environment will be unable to create a short circuit within the board. The error rate of the chipset per processor per day must be incredibly low, as the scientific data must be transmitted to the ground stations with great accuracy.

Tolerances on the capacity of the solid-state memory modules chosen for the spacecraft were computed using the worst-case buffer capacity requirement calculated in the payload section of 10 Gigabytes of data. MicroSat Systems, Inc, under a Missile Defense Agency contract, has developed a radiation-hardened solid-state memory array capable of operating in LEO at a capacity of 20 Gigabytes of storage space^[5]. This allows for a margin of safety of 2. The memory array discussed above is shown in figure 5.2. By combining this memory system with the developmental Dependable Multiprocessor the spacecraft would be able to achieve its processing requirements with excellent conservation of power through the utilization of innovative new technology.

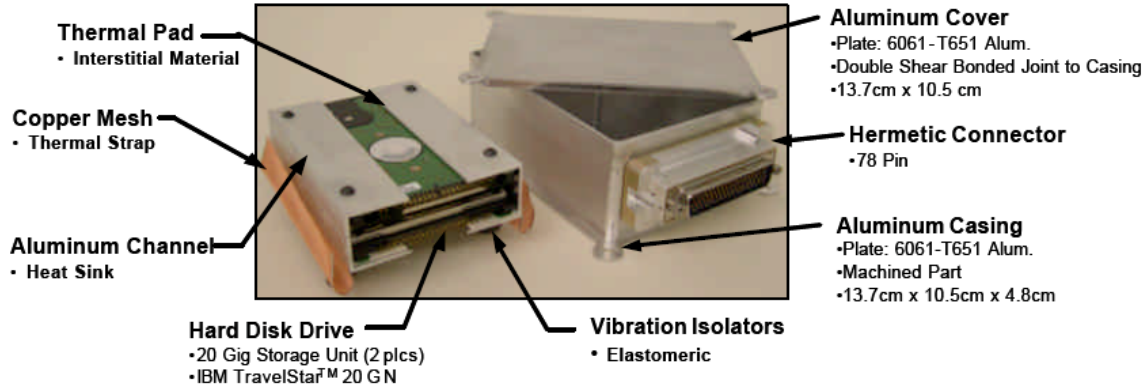


Figure 5.2: MicroSat Systems Inc. 20 GB SSD

8.3 Future Work

The computer system must be optimized and tested to levels far beyond the scope of this report for proper mass distribution and resistance to radiation in the environment of the low-earth orbit chosen in the mission analysis sub-section. Once the Dependable Microprocessor system is fully developed by Honeywell, Inc. its dimensions and true power requirements, as well as its thermal control requirements, would need to be factored into a full computational model of the system and tested for proper placement within the structure. As the memory capacities of solid-state drives increase, the memory budget for the spacecraft would need to be upgraded, as the limiting factor of computation on this spacecraft is the memory buffer. A larger memory buffer would allow for a camera with higher resolution than the thermal imager currently in use. A custom memory array or microprocessor would, of course, optimize the design still further, but, as mentioned above, the overall design requirements dictate the use of off-the-shelf components wherever possible to minimize non-recurring costs. The development of the memory array and microprocessor system is ongoing, but the design team is confident that the choices made within this subsystem will not need to be changed in the final implementation.

9 Communications

9.1 Overview and Requirements

The communications section will explore the data downlink and upload telemetry capability of the satellite. Several ground stations were chosen and the engineering link was developed. Minimum and average access times were tabulated and graphed, and the time between passes was also analyzed. In conjunction with the data from the Mission Analysis and Launch section, engineering budgets, data rates, and required gains were computed. Ground station constraints such as elevation angle are taken into account in choosing half cone angles for the antennas, and balancing trade offs between slant range, swath width, and time to global coverage. From this information we chose viable commercial antennas and transponders for the spacecraft.

9.2 Detailed Design

Engineering Communications Link

The satellite must be able to receive telemetry commands from Earth ground stations while also having the capability to quickly transfer large amounts of data. These requirements mean that the spacecraft must have both receiving antennas listening for commands as well as transmitters to relay data to the ground. Since the hard drive data storage capability of the satellite is limited, the data from the urban heat island measurements must be relayed to the ground in a timely and reliable fashion.

Calculating Half Angle, Slant Range and Swath Width

For a satellite with altitude h , earth radius R_E , and worst case elevation angle ε we can find the slant range R as

$$R = \sqrt{(R_E + h)^2 - R_E^2 \cos^2 \varepsilon - R_E \sin \varepsilon} \quad (9.1)$$

Thus, using $R_E=6378\text{km}$, $h=500\text{km}$ and assuming $\varepsilon = 10$ degrees for a typical ground station, we find that $R = 1695.08\text{km}$. Furthermore, we can solve for the half cone angle of the downlink with the formula

$$\gamma = \sin^{-1} \left(\frac{R_E \sin(90 + \varepsilon)}{h + R_E} \right) \quad (9.2)$$

which yields $\gamma = 65.95$ degrees for the downlink half cone angle. Using this figure in conjunction with the slant range, we can compute the swath width of the data downlink using the Pythagorean theorem (by ignoring the curvature of the Earth) to obtain

$$\frac{SW}{2} = \sqrt{R^2 - h^2} \quad (9.3)$$

Solving for SW, the swath width, yields 3239.3 km, roughly the distance of from the East to West coast on the United States; easily adequate enough for our needs. This antenna will then be used as both a transmitter and a receiver of data. Now that we have the basic specifications for the swath width, slant range and half angle, we can choose the ground stations for the spacecraft.

Ground Station Selection

Three ground stations were chosen to ensure that the data can be downloaded promptly and without costly delays between transmission times. The limited data storage capability of the satellite means that the information must be relayed to ground stations relatively quickly. We chose our ground stations locations to be in Boston, Anchorage, and Svalbard (Norway). While Boston and Anchorage are both relatively high latitude sites within the United States, we wanted a ground station that is truly high-latitude and would allow minimal time between access points. Instead of just picking a point on the North Pole, we wanted a location that could reasonable be used as a ground station. To achieve this, we searched for already existing high-latitude command and control centers. The best option was Svalbard Satellite Station (SvalSat),^[1] a ground station established in 1997 explicitly to provide support for polar orbiting satellites.

STK was then used to conduct a 5 day, 76 orbit simulation of access times to all three of the ground stations. We created a spacecraft with a noon-midnight sun synchronous orbit, added all three of the ground stations, and created a downlink with a 65.95 degree cone angle. The resulting 3D view and 2D ground tracks of the satellite are shown in figures 9.1 and 9.2. Figure 9.2 also shows typical ground tracks of a polar LEO orbit, as well as the ground station access zones in white for Boston, light green for Svalbard and forest green for Anchorage. In the simulation, the satellite was currently over the Atlantic. Figure 9.1 shows the satellite on a 3D map of the earth, as well as a line for its orbit and a purple cone for the communications link.

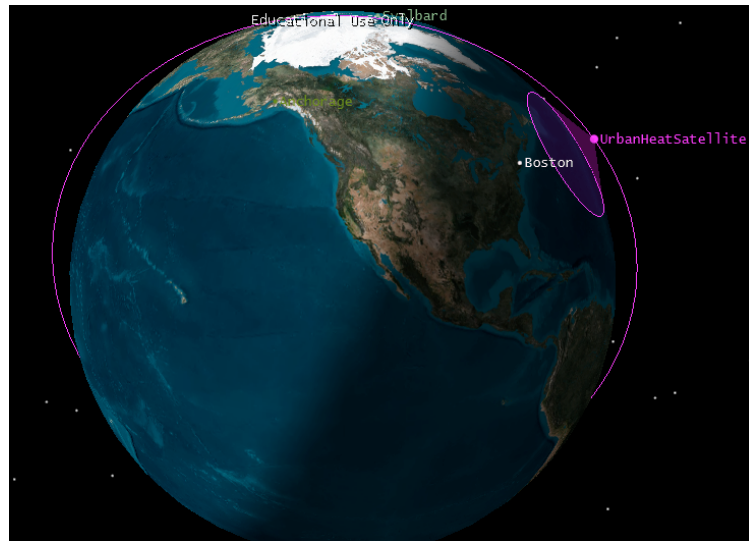


Figure 9.1: 3D View of Satellite and Swathe Area

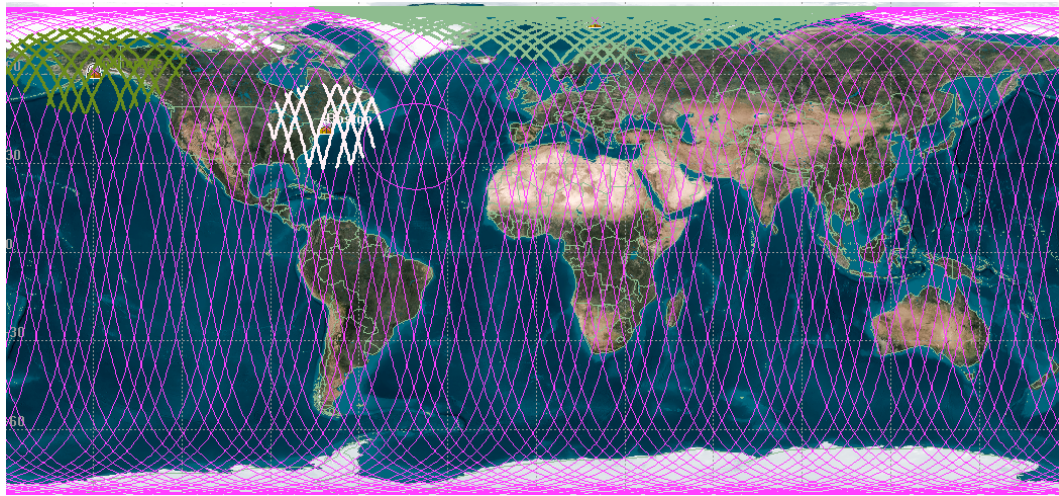


Figure 9.2: Satellite Ground Tracks and Ground Stations Access Zones

A report was then generated which shows the number of accesses, average access time, minimum access time and total access time to each one of the stations. The results are shown in Table 9.1, where the advantage of having a ground station in Svalbard becomes immediately clear; the total access time at this station is over 3.5 times as much as for Boston and over twice that of Anchorage, totaling about 5.88 hours over five days.

	Anchorage	Svalbard	Boston
Number of Accesses	28	54	17
Average Time, sec	349.22	391.84	346.94
Minimum Time, sec	123.05	106.40	82.91
Total Time	9778.11	21159.41	5897.93

Table 9.1: Spacecraft-Ground Station Access Times for a 5 day period

By computing the total amount of time passed in our STK simulation (5 days) and subtracting the total access time, we can find the total amount of time where we cannot access the ground stations with the high gain antennas. Dividing this figure by the total number of accesses during the simulation yields the average length of time between successive accesses. Additionally, inspection of access reports for all three of the ground stations yields the maximum time between passes. This data is tabulated in Table 9.2.

	Anchorage	Svalbard	Boston
Average Time	4.19 hours	2.11 hours	6.96 hours
Longest Time	11.30 hours	9.50 hours	11.53 hours

Table 9.2: Time Between Passes for Each Ground Station

In reality, we are also interested in how well the stations work together. That is, although it is useful to know what the time between accesses is for each individual ground station, it is more useful to know how long the gap may be between any two stations. Figure 9.3 graphically show the downlink access times to all three of the different ground stations. The short vertical lines represent times when there is access to one of the stations, and the

color indicates which station is being accessed. As the figure shows, there is some overlap in accesses and the time between successive accesses at ground stations is small.

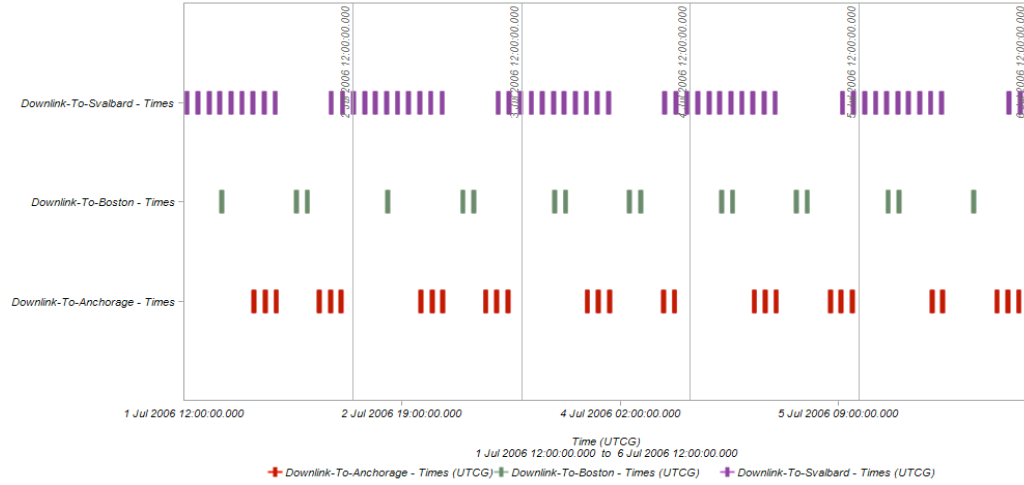


Figure 9.3: Graph of Downlink Access Times to Three Different Ground Stations

By inspection of Figure 9.3 and the access reports from STK, we can deduce that the maximum amount of time between 2 accesses of any ground station occurs between access at Anchorage and Boston during a gap in access to Svalbard during the last day. It should be noted that we assumed that Svalbard needs a minimum elevation of 10 degrees to get reliable data from the spacecraft; if it can accommodate smaller angles then we would have nearly continuous access to SvalSat. With the 10 degree minimum, however, the largest gap in access is computed to be 4 hours and 18 minutes.

Onboard Data Storage and Data Relay Capability

Since the satellite will experience some times when it cannot transmit to any of the ground stations, data storage and data relay capability will be very important. Although the longest that it should ever go without accessing a ground station is 4 hours and 18 minutes, we have designed the spacecraft to be able to store data for a longer period of time in case of emergencies. In addition to onboard data storage (see Computing Section), we thought it would be prudent to add an omni-directional antenna that can communicate at all times in the event of an emergency. In this scenario, the spacecraft could transmit data directly to NASA's Tracking and Data Relay Satellites (TDRS), which is a group of satellites in GEO orbit that provide global coverage of LEO satellites and relay information to a single ground station in White Sands, New Mexico. One potential problem with this solution, however, is that the majority of the Van Allen Belts lies between the LEO and GEO orbits, so that the signal must pass through a region with significant noise. However, given the correct modulation scheme and gain profiles we do not think this will prevent our spacecraft from transmitting clear signals in emergencies.

Data Rate, Signal Frequency and Link Budget

Assuming 2 pictures per city (one IR and one visible), and 15 cities per orbit, gives a total of 30 pictures taken in the 94 minute period, each 120MB in size, we have a total of 3600MB of data to download. However, since the spacecraft may take as long as 259 minutes, or 2.76 orbits between accesses, this means that we may have up to 9.94

gigabytes of data to downlink. Given the minimum possible access time for this scenario (445 sec), this corresponds to a maximum required data rate of 178.7 Mbps. However, taking a typical 1 orbit cycle (3.6GB of data), within the minimum possible time to downlink (82.91sec over Boston), we get a maximum data rate of 347.4 Mbps. To accommodate this data rate we would have to use an antenna in the X-band.

Next, we compute the equation for the link budget as

$$\frac{E_B}{N_0} = P_T + L_T + G_T + L_S + L_A + \frac{G_R}{T_S} + R + \text{Margin} \quad (9.4)$$

where P_T is the transmitter power, L_T is transmitter to antenna line loss, G_T is the gain of the transmitting antenna, L_S is the space loss, L_A is the transmission path loss, G_R is the receiving antenna gain, T_S is the system noise temperature, and R is the data rate. Typical link margins are 0.5 to 2.5dB and typical system noise temperature are 135K for downlink and 614K for uplink for a 2-12Ghz antenna.^[2] The path loss can be calculated in dB as $32.5 + 20\log(R) + 20\log(f)$.^[3] Other losses could include modulation loss, multipath loss and other miscellaneous losses. Lastly, the link margin is the difference between the theoretical Eb/No and the actual number, basically accounting for ‘implementation loss.’ This figure ranges from 0.5 to 2.5dB.^[4]

Equipment Selection

For the ground stations, Svalbard is already equipped with six antenna systems, including two 11 meter antennas and one 13 meter antenna. These antennas can download in S band and X band and upload in S band. For Anchorage and Boston, more research should be done to find if there are any existing satellite communications centers. If not, then a ground station should be set up with powerful antennas. One option would be to use 11m diameter antennas from Patriot or Andrew Corporation, with capabilities in the S band and X band.

The exact satellite antenna selection will depend on what is chosen for the ground stations. The most logical would be to use two S band antennas and an X band antenna. The two S bands would include one high gain receive and transmit antenna to communicate engineering data with the ground station and an omni-directional antenna to communicate with NASA’s TDRS in case of emergencies. A typical parabolic S band antenna operates at about 1.7Ghz, has a gain of about 16-19dBi, a beamwidth of approximately 18 degrees and a weight of 3.9kg.^[5] An omni-directional antenna typically operates in similar frequency ranges but have much lower gains and higher power requirements.

Next, we would use an X band transmitter for the science downlink to accommodate the higher data rate that is necessary for dumping the high resolution images. This antenna would have a frequency in the 7-8 Ghz range and a higher gain than the S band. Lastly, we would need one ore two transponders. Their role would be to send back a signal to the ground station, probably in S band, at a slightly different frequency then what was received to ensure receipt of the data.

9.3 Future Work

Several factors remain to be tweaked in this section. Most importantly, we must assess the viability of creating ground stations in Anchorage and Boston, as well as whether its within our budget to use SvalSat. Also, if SvalSat can actually obtain data from every single pass as it claims on its website (meaning it does not have a minimum 10 degree elevation limit), then it would drastically reduce the longest the spacecraft would have to go without dumping data. The figure would drop from about 3 hours to under 90 minutes. This would have implications for spacecraft computing and power.

Additionally, more research has to be done to make sure that the correct antennas were chosen for the communication link. Although it seems reasonable to use the same antenna for receiving and transmitting, a more thorough analysis should be conducted to confirm this. As always, cost optimization should be an important factor in the decision. Other things that must still be done include calculating a link budget, gains for the antennas, and power numbers for the entire communication system. Lastly, a modulation scheme should be designed for the task at hand.

10 Structures

10.1 Overview and Requirements

Developing an ideal structure for the spacecraft is an iterative process with many tradeoffs. The purpose of the structures is to encase and provide protection to the payload, while also serving as the mechanical interface with the launch vehicle. The mass distribution of the different subsystems within the structure is also very important to ensure stability. Additionally, instruments must have a clear field of view and thermal requirements must be satisfied. The optimization process involves minimizing mass, drag, axial load, later load, gravity loss and cost. Using lightweight, stiff materials is often a good way to achieve these goals. A simple performance index calculation is introduced to aid in materials selection for the spacecraft, and buckling, yield, and resonance frequency conditions were checked. A preliminary internal architecture was developed and secondary support structure analysis was introduced.

10.2 Detailed Design

Primary Structure

Several different types of structures can be used for the walls, including thin or thick walled tubing, I-beams, H-beams or angle construction.^[1] We will be using a sandwich construction for our spacecraft, which combines a honeycomb layer with adhesive and a face sheet on each side. This combination produces a lightweight, strong and stiff structure. A whole range of composite materials are available, and further research should be done to determine the best option, although graphite epoxy seems like a good first choice. The internal space should be reinforced with beams that have a high shape factor, such as an I-beam. These internal trusses must be strong enough to provide adequate support but also light enough to avoid breaking. One way to find a material that optimizes these metrics is to use a performance index. The objective function which maximizes stiffness and strength while minimizing density is defined as^[2]

$$M = \frac{E\sigma_y}{\rho^2} \quad (10.1)$$

A materials chart can be created for these conditions, and a material (probably an aluminum alloy) should be chosen to maximize the objective function. Once a material is chosen, several different analysis should be performed on the primary structure to ensure that it will maintain its structural integrity. First, a stress analysis should be conducted to ensure that the chosen material does not fail and reach critical stress. The magnitude of stress, σ , produced by moment M on a cross section with moment of inertia I , at distance y from the neutral axis is defined as:

$$\sigma = \frac{My}{I} \quad (10.2)$$

If the axial and transverse loading stresses can exist simultaneously, the worst-case normal stress is defined as the sum of these two stresses:

$$\sigma = \frac{P}{A} + \frac{M(h/2)}{I} \quad (10.3)$$

The above quantity is defined for a tensile stress, so that the stress would be -1 times (10.2) for a compressive stress. Next, analysis of buckling must be conducted to ensure that none of the structural supports, namely the internal support beams buckle under stress. The critical stress which causes buckling is defined as

$$\sigma_{cr} = \frac{C\pi^2 E}{(L/\rho)^2} \quad (10.4)$$

where C is a constant dependent on the end boundary conditions, E is the elastic modulus (Young's modulus), L is the column length, and ρ is the radius of gyration of the cross section, equal to $\sqrt{\frac{I}{A}}$. Additionally, the concepts of factor of safety and margin of safety should be used in the design. Factor of Safety, (FAS), is defined as the load that causes failure divided by the expected load; this number is typically between 1.25 and 1.4.^[3] The margin of safety, MOS, is defined as

$$MOS = \frac{AllowableLoad}{ActualLoad * FOS} - 1 \quad (10.5)$$

Secondary Structures

The secondary structures include the solar panels, the AIRS (atmospheric spectrometer), the pushbroom imager, and the antennas. The solar panels are typically mounted opposite one another to maintain principal moments of inertia for the satellite. Keeping the mass distribution even helps with attitude dynamics and control, so it is an essential part of the design. Since the exact power requirements of the spacecraft, and hence the optimal size of the solar panels, is not yet known, their optimal position cannot yet be determined. The omni-directional antenna should be mounted facing towards NASA's Tracking and Data Relay Satellites, while the S-band antenna and X-band antenna for the engineering and science downlinks, respectively, should be pointed at the Earth. Special attention should be given to ensure that the hydrazine thrusters used for attitude control do not interfere with AIRS and the imager. Analysis of the fuel tanks is also important to ensure that they do not fail when pressurized; this analysis was completed in the Propulsion section of the report.

Internal Architecture

The internal architecture refers to the optimization of space within the satellite structure. The entire power subsystem, including the bus, batteries, and wiring to the payload, communications system, and attitude control subsystem is housed within the structure. The thermal system, including the heat pipe, is also housed within this structure and an

optimization should be performed to ensure optimum mass and space distribution. Since this is only a preliminary proposal and dimensions are uncertain, this is left to future work.

Acoustic Analysis and Margin of Safety

The spacecraft is exposed to a variety of acoustic disturbances throughout its mission. These include the initial rattling around during launch, the separation from the fairing, spin stabilization, and then all the perturbations that could occur during operation. A general rule used in structural design is the octave rule, which states that the component natural frequency must be over twice the natural frequency of the mounting or support structure. The natural frequency of the spacecraft must thus be computed, and an analysis should be completed to ensure that no perturbations cause this exact frequency to be induced within the structure.

10.3 Future Work

Since much of the analysis for structures depends on optimizing quantities dependent upon mass, geometry, (and thus moment of inertia), power usage, and other material properties, only the theoretical framework was given in this section. Much future work still remains to be done, especially on the internal architecture and materials selection fronts. Topics such as fuel slosh, shear stress conditions, precise moment of inertia calculations, performance index analysis for all materials, finite element structural analysis, thermal stresses and acoustic stresses should all be addressed.

11 Thermal Design

11.1 Overview

The thermal system is responsible for maintaining a thermal environment within the spacecraft that takes into account the individual tolerances of all of the instrumentation chosen for the mission. Each instrument has its own unique set of tolerances, and each active component by definition contributes an internal source of heat to the system. The sun also heats the system on one side, creating a temperature gradient across the entire spacecraft body. The thermal system is especially complex when presented with non-steady-state occurrences such as eclipses—active methods of heat control must be designed to account for such events.

This section will examine the various considerations and calculations integral to the design of a well-functioning thermal control system and select methods of passive and active thermal control relevant to the mission and will provide the outline of a full thermal analysis. The following will examine the various steps that must be taken by an expansion of this report to characterize the thermal environment of the spacecraft.

11.2 Detailed Design

The first step in the detailed design of the thermal environment on board the spacecraft is the achievement of an in-depth understanding of the various heat fluxes incident on the system in the LEO environment. A full analysis would provide a list of heat tolerances for the specific components decided upon in the previous sub-sections, but such detail is beyond the scope of this report. The following will examine the various steps that must be taken by an expansion of this report to characterize the thermal environment of the spacecraft.

The three main types of heat flux expected to act upon the spacecraft come from solar radiation, earth's infrared emissions, and the earth's albedo, or reflected solar light. These fluxes are defined respectively in equations 11.1, 11.2 and 11.3 below:

$$Q_{\text{sun}} = \sigma A_s F_{s-\text{sun}} T_{\text{sun}}^4 \quad (11.1)$$

$$Q_{\text{earth}} = \sigma A_s F_{s-\text{earth}} T_{\text{earth}}^4 \quad (11.2)$$

$$Q_{\text{alb}} = Q_{\text{sun}} \rho_{\text{alb}} \phi_1 \cos \phi_2 A_s F_{s-\text{planet}} \alpha_{ss} \quad (11.3)$$

Calculation of these values is dependent on a greater knowledge of the spacecraft structure than was reached in this report. In addition to these external fluxes an internal flux would be generated within the spacecraft by the ADC system and other powered components. This flux must be factored in to the analysis.

If the aforementioned model of the full spacecraft outlined in the sections above existed in a program such as Pro/E with a thermal analysis program, the conductivities through and across the spacecraft's external panels could be calculated. The entire spacecraft could then, for the purposes of this analysis, be approximated as a solid slab with the conductivities calculated above. A temperature gradient would then be

calculated by setting the fluxes across the surfaces in equilibrium—in effect, by setting the heat flux into the system equal to the heat flux out of the system. As discussed in Pisacane's *Fundamentals of Space System Design*, the heat flux out of a spacecraft can be approximated as a black body emitting radiation at a specific temperature. By setting this black body radiation equal to the sum of the fluxes discussed above, a temperature gradient could be calculated across the spacecraft. The two equations that must be solved for are listed in equations 11.4 and 11.5 below:

$$\frac{Q_{\text{incident}}}{A} = \epsilon \sigma T^4 \quad (11.4)$$

$$\frac{Q_{\text{incident}}}{A} = \frac{k \Delta T}{L} \quad (11.5)$$

where Q_{incident} is the sum of heat fluxes, A is the surface area, ϵ is the emissivity, σ is the Stefan-Boltzmann constant, k is the conductivity of the spacecraft, and L is the length of the spacecraft along with the temperature gradient occurs. This temperature gradient could then be applied to the thermal analysis model within Pro/E to find the specific thermal environments around each component. As mentioned above, a full analysis would include tolerances for each component and take the specific necessary steps to cool or heat each component and keep it within these tolerances for a variety of spacecraft modes including eclipse, launch and steady-state operation.

Given the data from such a detailed analysis, passive and active control schemes must be decided upon with the overall goal of drawing heat from the surfaces on which the flux acts to the dark surfaces facing away from the sun. By minimizing the thermal gradient on the system with passive control methods, the active control methods discussed below will require far less power and will be far easier to tailor to specific components in a predictable fashion.

Options for passive control of the thermal environment include modification of the surfaces of the spacecraft to change the emissivity properties, and the inclusion of passive devices within the structure, such as heat pipes. Optimal passive thermal control can be achieved through a black color scheme, allowing maximum absorption of heat by the spacecraft, and some sort of sheeting on which the color scheme is applied that minimizes the emissivity of the spacecraft. The passive control system was designed with the aim of retaining as much heat from the incident fluxes as possible, as heat is far less costly to get rid of than the generate—once this heat is retained, heat pipes will be used to route heat throughout the structure, if the analysis shows that not enough heat is reaching the back of the spacecraft. The heat pipe routes far more wattage than the structure itself, and the addition to the mass budget and the effect on structural integrity of the spacecraft is far less of a concern than the benefits conferred by the pipes.

If the system were always to run in a steady state environment, passive control would be enough to ensure an acceptable thermal environment. However, as discussed above in the attitude determination and control subsection, multiple modes of operation must be accounted for to deal with eclipses and the launch environment (to make sure that all components stay within their failure limits for temperature). During an eclipse cooling occurs from all surfaces of a spacecraft—analysis must be done to ensure that no

components fall below minimum temperature during this time. Heating tape would help correct for this, and would allow the application of small fluxes directly on structural areas that needed thermal assistance.

11.3 Summary and Future Work

Based on the above discussion of the steady-state environment within the spacecraft, this section laid the groundwork for calculation of the average temperature that could be maintained given the incident heat fluxes on the system. The use of heat pipes or other passive thermal controllers to transfer heat from the spacecraft surfaces exposed to the sun back to the unheated surfaces on the opposite side will decrease the natural temperature gradient and push each element of the system as close to average as possible without significantly increasing the mass of the spacecraft.

Further work must be done on thermal analysis for the spacecraft's non-steady-state modes, such as heat exchange in the launch environment and during non-steady events such as eclipses. At launch, the system's thermal environment does not need to fall within operational range, as each system will lie dormant until the final orbital altitude is reached and orbit is established, but the failure temperatures for each instrument and system must be considered, as the launch window contains the most extreme thermal states that the spacecraft will experience.

The thermal environment and cooling effects during eclipse, or satellite safe mode, must be examined in far greater depth to allow for proper design of active control systems, such as heat tape combined with thermocouples for local temperature measurements, and for precise application of these systems at necessary points within the spacecraft structure. Extra passive thermal protection, such as insulation, might be deemed necessary for certain components during non-steady events—these components would then need to be cooled during steady-state operation.

12 Conclusion

The design of the Hephaestos UHI Monitor was a rewarding experience that taught the design team much about the discipline and the intricacies involved in creating a system capable of functioning in a LEO environment over a realistic lifecycle. Though the scope of this report was too small to present a design evolved past the preliminary state, all of the goals laid out above in the systems overview were met, and it is the opinion of this team that with further research the Hephaestos spacecraft could be made operational given current technology. The problem of climate change is proving to be one of humanity's most pressing concerns over the coming decades. As a method of feedback on the efforts of humankind to mitigate the species' effect on the heat signature of the planet, Hephaestos and other initiatives of its kind are invaluable.

For each system, the work required to develop concept into reality is roughly equivalent. In-depth analysis within Pro/E and STK is necessary to determine the specific analytical forces on each component and subsystem, as well as on the full spacecraft, before true design decisions on componentry can be made. The section on thermal analysis in particular must be expanded to make sure that the selected componentry can function at all within the LEO environment.

After the final components are chosen a mass budget must be assembled and a volumetric analysis of the internal space of the Hephaestos spacecraft must be completed so that each component can be appropriately placed within the structure. Once a mass budget exists and a full 3-dimensional model has been created within a computer, a serious attempt could begin to select a suitable launch vehicle and raise money for actual physical testing of the spacecraft. This report puts the Hephaestos project quite far down this timeline towards an actual realization of the concept.

Appendix A: Sources

A.1 References

- Pisacane, Vincent L. *Fundamentals of Space Systems*. Oxford: Oxford University Press, 2005.
- Sutton, George P. *Rocket Propulsion Elements*, 7th edition. Hoboken: Wiley-Interscience, 2000.

A.2 Notes

1. Introduction

- [1] http://en.wikipedia.org/wiki/Urban_heat_island
- [2] http://en.wikipedia.org/wiki/Urban_heat_island
- [3] http://en.wikipedia.org/wiki/Urban_heat_island
- [4] http://en.wikipedia.org/wiki/Urban_heat_island
- [5] <http://www.epa.gov/hiri/about/index.html>
- [6] http://en.wikipedia.org/wiki/Urban_heat_island

3. Payload

- [1] <http://www-airs.jpl.nasa.gov/Technology/>
- [2] <http://www-airs.jpl.nasa.gov/Technology/>
- [3] <http://www-airs.jpl.nasa.gov/Technology/>
- [4] <http://www-airs.jpl.nasa.gov/Technology/>

4. Mission Analysis & Launch:

- [1] Charles Brown, *Elements of Spacecraft Design*
- [2] http://en.wikipedia.org/wiki/Polar_Satellite_Launch_Vehicle
- [3] http://en.wikipedia.org/wiki/Polar_Satellite_Launch_Vehicle
- [4] http://en.wikipedia.org/wiki/Polar_Satellite_Launch_Vehicle

5. Propulsion

- [1] http://en.wikipedia.org/wiki/Cold_gas_thruster
- [2] Pisacane, *Fundamentals of Space Systems*, 259-260
- [3] http://cs.astrium.eads.net/sp/SpacecraftPropulsion/Propellant%20Tanks/Bladder_Tanks.html
- [4] <http://en.wikipedia.org/wiki/Hydrazine>

6. Power

- [1] Pisacane, Vincent. *Fundamentals of Space System Design*, p 330
- [2] Danielak, Robert. Lockheed Martin Class Presentation Slides on EPS
- [3] Danielak, Robert. Lockheed Martin Class Presentation Slides on EPS
- [4] Pisacane, Vincent. *Fundamentals of Space System Design*
- [5] Pisacane, Vincent. *Fundamentals of Space System Design*
- [6] Pisacane, Vincent. *Fundamentals of Space System Design*

7. Attitude Determination and Control

- [1] http://en.wikipedia.org/wiki/Reaction_wheel
- [2] http://books.google.com/books?id=31GqndM3fk8C&pg=PA347&dq=solar+radiation+torque&ei=CBYnSMKIKJzkyAS6hd2RCw&client=firefox-a&sig=_rQ_V3dt4zABgzX8cFYT5BjjYjU#PPA347,M1
- [3] <http://en.wikipedia.org/wiki/Quaternions>

8. Computers and Software

- [1] http://en.wikipedia.org/wiki/Million_instructions_per_second
- [2] Harris CrossStar Manual
(http://www.govcomm.harris.com/solutions/downloads/datasheets.asp?cat_id=107)
- [3] <http://nmp.nasa.gov/st8/>
- [4] http://nmp.nasa.gov/st8/tech/eaftc_tech3.html
- [5] MicroSat Systems Memory Array Paper (<http://www.microsatsystems.com/>)

9. Communications

- [1] <http://www.ksat.no/Products/Svalsat.htm>
- [2] Stengel, Robert. Class Lecture Notes
- [2] Pisacane, Vincent. *Fundamentals of Space System Design*
- [3] Stengel, Robert. Class Lecture Notes
- [3] Stengel, Robert. Class Lecture Notes

10. Structures

- [1] Pisacane, Vincent. *Fundamentals of Space System Design*
- [2] Ashby, Michael. Materials Selection in Engineering Design
- [3] Stengel, Robert. Class Lecture Notes.

Appendix B: Propulsion

B.1 Thruster Spec Sheet

1 N HYDRAZINE THRUSTER Model CHT 1

Characteristics	
Propellant	Hydrazine
Inlet Pressure Range	5.5 to 22 bar
Thrust Range vac	0.320 - 1.1 N
Isp vac	200 to 223 sec
Total Impulse	112,000 Ns
Cycle Life	59,000 cycles
Propellant Throughput	52 kg
Accumulated Burn Life	50 hours
Minimum Impulse Bit	0.01 - 0.043 N
Overall length	172 mm
Nozzle diameter	7.6 mm
Mass:	0.29 kg

[More information](#) and [Heritage](#)

A non-ITAR design is also available, fully qualified with European Flow Control Valve, Catalyst Bed Heater and Temperature Sensor.

Status: Readily Available

Further views of the 1 N hydrazine thruster - click to enlarge.



[CHT 1 N with i/f mount](#)



[CHT 1 N with i/f mount](#)



[CHT 1 N Leak Checking](#)



[CHT 1 N](#)

(Figure taken from
<http://cs.astrium.eads.net/sp/SpacecraftPropulsion/MonopropellantThrusters.html#CHT1>)

B.2 Propellant Tank Spec Sheet

VISIT US ON OUR WEBSITE @ WWW.PSI-PCI.COM

TANK TYPE Diaphragm	MOUNT Lugs (2)	LOCATION Girth	ATK PSI PRESSURE SYSTEMS INC
This is a 19-inch propellant tank is a spherical pressure vessel constructed of 6AL-4V Titanium. Positive propellant expulsion is provided by a reversing AF-E-332 rubber diaphragm retained at the sphere mid-plane. Mounting is accomplished by lugs parallel with and adjacent to the mid-plane. Connection is made to the propellant and pressurant compartments through tube stubs.			ATK Part Number 80486-1 SIZE: 19.06 -inch ID Sphere SIZE: 484-mm ID Sphere
ISO 9001 & AS 9100 REGISTERED			
APPLICABLE DOCUMENTS Acceptance Test Procedure 50-000671 Cleaning CPP 3995			TANK CHARACTERISTICS
DIAPHRAGM INFORMATION Diaphragm P/N 60-274007-1 Diaphragm Mold P/N T-1981 Diaphragm Gross Wt 1.71 Diaphragm Matl Type AF-E-332 Diaphragm, Material 90-000075 Diaphragm Processing 90-000079 N-Ray Inspection Procedure 1002			ACCEPTANCE TESTS Preliminary Examination of Product Pre-Proof Volume Determination Proof Pressure Test Post-Proof Volume Determination Pressure Differential & Expulsion Efficiency Penetrant Inspection* Radiographic Inspection* Internal Leakage Test External Leakage Test Determination of Weight & Final Inspection Cleanliness Verification Final Visual Examination
TANK CHARACTERISTICS (Metrics) Operating Pressure, Bar 25.99 Total Volume, l 59.50 Proof Pressure, Bar 34.34 Prop Volume, l 45.03 Cryo Proof, Bar No Max Design Wt, Kg 6.01 Design Burst Pressure, psig 754 Minimum Wall, Inch 0.023 Actual Burst Pressure, psig			
FORGINGS Notes: 1: Tube protector is SK 1476-1 FORGINGS P/N SUPPLIER Die 60-162061-1 (2)			QUALIFICATION TESTS Qual was performed on 80274-1.
Ring Size, (Rough Machined) Ring Forging SIZE 60-274065-1, Retainer 19.03 + .12 OD x 17.55 - .12 ID x 1.5 + .12 Lg 60-274063-1, Lug 21.25 + .06 OD x 19.31 - .06 ID x .85 + .06 Lg			VACUUM RATED YES
TUBE TYPE AND SIZE TITANIUM SIZE 60-486015-3 .250 OD x .020 Wall			
TUBE TYPE AND SIZE (Metrics) TITANIUM SIZE 60-486015-3 6.35 x .5 MM Wall			
			
23-Jun-04		6033 East Bandini Boulevard Commerce, California 90040	
		Telephone (323) 722-0222 Facsimile (323) 721-6002	

(Figure taken from http://www.psi-pci.com/Data_Sheet_Index_Diaphragm-PN.htm)